RSC Advances

REVIEW

View Article Online
View Journal | View Issue

Cite this: *RSC Adv.*, 2026, **16**, 4898

Recent advancement in ZnAl-LDH-mediated systems towards photocatalytic energy and environmental applications and piezo polarized photocatalytic reactions: synthesis to application *via* mechanistic insights

Naisargika Mallick,† Susanginee Nayak, † Anshumika Mishra, Upali Aparajita Mohanty and Kulamani Parida *

ZnAl-layered double hydroxide (ZnAl-LDH) is an emerging robust material that has attracted great attention in the field of photocatalysis and piezo polarization-induced photocatalysis owing to its unique physicochemical properties, including a high specific surface area, tunability in metal cation dispersion, specific catalytic site placement, rapid response to mechanical stress, stability, and environmental-friendliness. However, pristine ZnAl-LDH showed low exciton pair separation efficiency, and low conductivity due to a wide band structure that limits their catalytic efficiency. Modifying the ZnAl-LDH-based materials by adopting various design strategies to form a composite or heterostructure ensures improved surface properties for better catalytic performance, stability, and efficiency. This review emphasizes the recent advancement towards designing ZnAl-LDH-based high-performance catalysts using adopted modification strategies such as doping or defect engineering, interlayer anion modification, structural modulation, heterostructure or composite formation, *etc.*, for improved activity. ZnAl-LDH-based high-performance catalysts boost structural adjustability, stability, and improved conductivity, exposing more active sites, thereby enhancing the catalytic performance. Hence, this review delivers a deep dive into the prospects of ZnAl-LDH-based high-performance materials for photocatalytic water splitting, pollutant degradation, CO_2 reduction, and piezo-polarized induced photocatalytic pollutant degradation. Furthermore, the progression of ZnAl-LDH-based high-performance catalysts with a detailed analysis of best-suited characterization techniques has been systematically reviewed to validate the structural characteristics of high-performance catalysts. The mechanisms described in the photocatalytic processes are also thoroughly reviewed. Lastly, the review highlights the advantages, challenges, and compliance perspective in designing ZnAl-LDH-based high-performance photocatalysts for energy production and environmental applications. This review serves as a gateway for exploiting ZnAl-LDH as components to design advanced catalytic materials for future energy safety and ecological deliverance.

Received 11th December 2025
Accepted 6th January 2026

DOI: 10.1039/d5ra09591c

rsc.li/rsc-advances

1. Introduction

The rising demand for high-value chemicals and energy to sustain modern society has inevitably increased the use of limited non-renewable fossil fuels. The excessive carbon emissions from burning fossil fuels have led to energy shortages and serious climate impacts, especially global warming and greenhouse gases.[1] Industrialization is the main source of water and environmental pollution, releasing pollutants such as dyes, organic chemicals, antibiotics, and pesticides. These harmful substances negatively affect human health and the environment.[2] Therefore, there is an urgent need for water treatment, air purification, and renewable energy solutions for sustainable global development. In this context, advanced oxidation processes (AOPs) have emerged as a highly environmentally promising and cost-effective technique for addressing persistent environmental remediation and clean energy generation issues.[3,4] These processes rely on the *in situ* generation of reactive oxygen species (ROSs), particularly $^{\bullet}OH$ and $O_2^{\bullet-}$, that can selectively degrade a wide spectrum of organic and inorganic contaminants as well as lead chemical reactions towards energy generation solutions. These processes offer efficient and

Centre for Nano Science and Nano Technology, Institute of Technical Education and Research (ITER), Siksha 'O' Anusandhan Deemed to be University, Bhubaneswar-751030, Odisha, India. E-mail: kulamaniparida@soauniversity.ac.in; paridakulamani@yahoo.com; Fax: +91-674-235064; Tel: +91-674-2351777

† Contributed equally to this manuscript.

robust, non-selective oxidation pathways for the mineralization of complex and recalcitrant contaminants in wastewater and industrial effluents into harmless end products like water and carbon dioxide, outperforming conventional treatment methods.[5] Simultaneously, their application in energy-related systems – such as photocatalytic water splitting and solar-driven hydrogen peroxide production – highlights their dual role in promoting sustainable water treatment and renewable energy development.

AOPs are central to advancing both environmental and energy technologies in alignment with green chemistry principles. Among various emerging AOP technologies, semiconductor-based photocatalysis showcases a promising environment-friendly approach to address energy and environmental challenges by utilizing abundant solar energy.[6] The photocatalytic process involves three key steps: light absorption to generate e^-/h^+ pairs, separation and movement of charges from the core to the surface, and activation of redox reactions and interfacial oxidation at the surface. Developing stable and efficient photocatalysts with suitable structures is crucial for practical applications. Several 2D semiconductor materials, such as MXene,[7] $LaFeO_3$,[8,9] graphitic carbon nitride (g-C_3N_4),[10,11] titanium dioxide (TiO_2), transition metal dichalcogenides (TMDs),[12,13] cadmium disulfide (CdS),[14] and metal–organic frameworks (MOFs),[15,16] are being explored. However, many of these have limited stability and photocatalytic activity for industrial use. Recently, Layered Double Hydroxides (LDHs) have gained increasing attention in the photocatalysis arena owing to their customizable composition and distinctive two-dimensional (2D) structures.[17] These materials are promising owing to their high specific surface area (SSA), unique layered architecture, ability to absorb light across various compositions, large interlayer spaces for creating composites with different functional species, extensive surface-active regions, ion-exchange capabilities, adjustable bandgaps, low cost, ease of scaling up, and reusability.[18,19] Besides, the photocatalytic performance of LDHs can also be improved by enhancing matrix flexibility, modifying cationic species, intercalating anionic structures, and forming heterojunctions with other semiconductors.[20] However, incorporating transition metal cations with different valence states alters the chemical environment and electronic structure within the LDH layers, which can influence the photocatalytic performance.[21]

Among all other LDHs, Zn-based LDH materials, especially ZnAl-LDH, merely debuted as a promising candidate for photocatalytic applications due to their several distinct advantages, including surface stability, superior dispersion of metal elements, atomic diffusion, and crystal lattice expansion. Additionally, ZnAl-LDH acts as a piezoelectric catalyst with considerable potential for environmental remediation due to its rapid response to mechanical stress and its affordable and eco-friendly nature. The density functional theory (DFT) studies of ultrathin ZnAl-LDH also reveal that defect structures composed of unsaturated zinc coordination and oxygen vacancies (O_Vs) can enhance the photocatalytic efficiency of these materials. In ZnAl-LDH, ZnO_6 octahedral units are dispersed on their surface, creating structural defects that trap electrons during photoactive reactions. Despite these advantages, ZnAl-LDH suffers critical challenges, including poor visible-light absorption, poor efficacy for charge segregation, and rapid exciton recombination, which limit their catalytic performance. To address these challenges, current studies are centered on research focused on the development of ZnAl-LDH-based hybrid materials by coupling them with other functional materials, carbonaceous materials, or plasmonic materials, *via* doping, defect engineering, heterostructure formation, derived products, and interlayer modification for modulating interfacial charge transfer, and bandgap tuning through mechanisms like type-II, Z-scheme, and S-scheme junctions.[22,23] This review systematically addresses the recent progression in ZnAl-LDH-based hybrid materials, highlighting the structure–property relationships and mechanistic aspects for improved photocatalytic efficiency. Besides, we have also tried to emphasize and highlight the emerging piezo-potential-enhanced photocatalytic field based on ZnAl-LDH systems.

Several review articles have thoroughly discussed LDH synthesis, properties, modifications, and applications across various technological fields. Notable progress has been made in engineering LDH-based photocatalytic systems to boost their performance. For instance, Bobde and his team developed LDH-based photocatalysts for dye degradation, focusing on system stability.[24] Song *et al.* demonstrated that the thoughtful design of 2D/2D LDH/g-C_3N_4 hybrid structures improves charge separation and light absorption, thereby increasing photocatalytic activity.[25] Tailored modification strategies have further advanced CO_2 adsorption and photoreduction, emphasizing the tunable surface chemistry of LDH nanostructures.[3] The photocatalytic behaviour of these materials is heavily influenced by vacancy sites, interfacial adsorption dynamics, and catalytic activity at metal/LDH heterojunctions.[26] Interfacial engineering has become a key approach for building efficient heterostructures with improved charge transfer pathways.[27] Additionally, advanced modification methods—such as surface plasmon resonance enhancement, co-catalyst addition, and composite development—have led to significant improvements in hydrogen production performance.[28] LDH-based semiconductors continue to show great potential in photocatalytic, electrocatalytic, and photoelectrocatalytic applications.[29] Furthermore, our group has contributed reviews in this area. For example, S. Nayak *et al.* summarized how structural tuning of LDH/GO hybrids has enabled the creation of hierarchical porous networks that facilitate efficient water-splitting reactions.[30] In addition, optimizing structural and electrical properties has further enhanced the photoactivity of LDH compounds,[31] and the use of first-row transition-metal LDHs as electrocatalysts has opened new pathways for overcoming operational challenges and increasing overall catalytic efficiency.[32]

While several reviews have broadly addressed design and modification strategies of LDH-based semiconductors, a focused analysis on ZnAl-LDH hybrids for photocatalytic applications remains limited. This review aims to bridge that gap by summarizing recent advances in doped, intercalated, and heterostructured ZnAl-LDH systems for pollutant

degradation, hydrogen evolution, CO_2 reduction, and piezo-potential-enhanced photocatalysis. Unlike existing overviews, it provides a detailed discussion on charge transfer mechanisms—including type-II, Z-scheme, and S-scheme pathways—as well as the roles of interlayer anions and O_Vs in enhancing activity. Emphasis is also placed on structure–property relationships and mechanistic insights, with particular attention to the emerging field of piezo-assisted photocatalysis based on ZnAl-LDH, which remains underexplored in prior literature.

Hence, in this review, firstly, we discuss the structure and properties of LDHs, focusing specific attention on ZnAl-LDH-based semiconductors. Several synthetic strategies have been highlighted to create modified ZnAl-LDH with substantial physico-chemical attributes and mechanisms, to precisely engineer their broad band gap for efficient visible light harvesting. Following this, an attempt is made to encapsulate the overview of fundamental design concepts of ZnAl-LDH-based high-performance catalysts and their application towards photocatalytic pollutant decomposition, CO_2 reduction, and hydrogen production by H_2O splitting reaction. Specific attention has been given to effective modification and engineering aspects, such as defect formation, interlayer tuning, doping for band gap engineering, and hetero-structure formation. Also, we have included how piezo-polarization causes a shift in surface charge energy and segregation of charge carriers at the bulk and interfacial area, which results in efficient exciton transfer, augmenting the photocatalytic pollutant degradation application. Lastly, the shortcomings and future perspectives are addressed to provide insights into shedding light on the design and tuning of the wide band gap of modified ZnAl-LDH-based nano-photocatalysts towards solar energy applications. Therefore, we anticipate that this review can serve as a roadmap for researchers to innovate a prospective towards modified ZnAl-LDH-based functional nanomaterials that integrate photocatalytic and piezo-catalytic characteristics to boost solar energy applications. Different research work integrating the growth trend of modified ZnAl-LDH for photocatalytic and piezo-polarized photocatalytic applications has been portrayed in Scheme 1.[33–41]

2. Fundamentals of LDH

Layered double hydroxides (LDHs), also referred to as hydrotalcite, are 2D lamellar ionic clay complexes having the basic formula $[M^{2+}_{1-x}M^{3+}_{x}(OH)_2][A^{x/n}]^{n-}\cdot mH_2O$. These composed of positively charged, brucite-like layers (brucite: $Mg(OH)_2$-type structure) that contain divalent cations ($M^{2+} = Zn^{2+}$, Fe^{2+}, Cu^{2+}, Co^{2+}, Ni^{2+}, *etc.*), trivalent cations ($M^{3+} = Al^{3+}$, Mn^{3+}, Cr^{3+}, Ga^{3+}, *etc.*) including interlayer charge balancing organic/inorganic anions ($A^{n-} = {CO_3}^{2-}$, ${SO_4}^{2-}$, Cl^-, porphyrins, *etc.*) along with H_2O molecules for structural stabilization. The cation ratio 'x' = $M^{3+}/(M^{2+} + M^{3+})$ ranges between 0.2 and 0.4, altering the layer charge density of the LDHs layers.[17,42,43] The positively charged brucite-like layers are made up of edge-sharing octahedral units $[(M^{2+}/M^{3+})\cdot(OH)_6]$ with metal cations arranged in the centres and six-fold coordinated OH^- ions surrounding each cation oriented toward the corners, forming infinite layers. The M^{2+} and M^{3+} ions alternately reside in the octahedral sites in LDHs, generating hydroxide layers that are stacked *via* van der Waals interactions.[28] Surface –OH groups in LDHs contribute to the formation of highly energetic radicals and metal-to-metal charge transfer (MMCT): denoting the electronic transition that arises from one metal to the other, and ligand-to-metal charge transfer (LMCT): associated with the electronic transition (from the oxygen 2p orbital to the 3d orbitals of metal centre) *via* oxo-bridged (M–O–M) bimetallic linkage, enabling electron migration that is crucial for photocatalytic applications.[18,20,28]

2.1. Structure and properties of ZnAl-LDH

In this regard, the tunability of M^{2+}/M^{3+} by altering the molar ratio in the layers that resemble brucite and the intercalated anions' exchangeability controls the physico-chemical and electronic properties of the LDHs materials.[21] The morphological and structural transformations of the LDHs material, such as exfoliation and reconstruction *via* "memory effect," expand surface area, size for enhanced photocatalytic activity.[17] The "structural memory effect" is a unique property of LDHs where the original LDHs structure is reconstructed by the hydration of calcined LDHs, which is used to synthesize LDHs-based composite photocatalysts. In ZnAl-LDH, zinc (Zn) is a prominent photosensitive metal included as Zn^{2+} into the brucite-like layer due to its ability to enhance solar absorption and promote charge separation. However, Foschini *et al.*, revealed that a greater Zn^{2+} ionic radius (74 Å) facilitates crystal lattice expansion, fostering atomic diffusion and pore volume. Though the optimal Zn^{2+} content in ZnAl-LDH rises pore volume up to 1.05 $cm^3\ g^{-1}$, significantly improving photocatalytic activity by offering numerous catalytically active sites. ZnAl-LDH produces mixed metal oxides (MMOs) as $ZnO/ZnAl_2O_4$ when calcined, facilitated by the tunability of interlayer species and metal composition that enhances photocarrier dynamics.

This transformation enhances catalytic activity by improving crystallinity, electron mobility, and solar absorption while reducing charge carrier recombination and layer aggregation that confirmed by photoluminescence (PL) analysis, thereby making the material an excellent and adaptable photocatalyst. Moreover, ZnAl-LDH-based MMOs can regain their original structure through rehydration known as "memory effect" which improves energy conversion by promoting charge separation due to better dispersion of the active phase from calcination. The PL analysis also confirms that their structural reconstruction reduces electron–hole recombination, augmenting photocatalytic performances. Veisi *et al.* demonstrated that on calcinated ZnAl-LDH at 450 °C transforms it into a $ZnO/ZnAl_2O_4$ composite facilitates better photocarrier transfer, reduces charge transfer resistance, and improves charge separation, and enables superior photocatalytic efficacy that outperforms its parent compounds.[44] In addition, these ZnAl-LDH derived ZnO phase may serve as effective photocatalysts for removal of a diverse array of organic waste due to their appropriate band gaps, and valence band edges (VB: +3.62 V *vs.* NHE at pH 0), which assist in the production of reactive species ($^{\bullet}OH$, $O_2^{\bullet-}$) for advanced oxidation. The derived ZnO phase get activated when

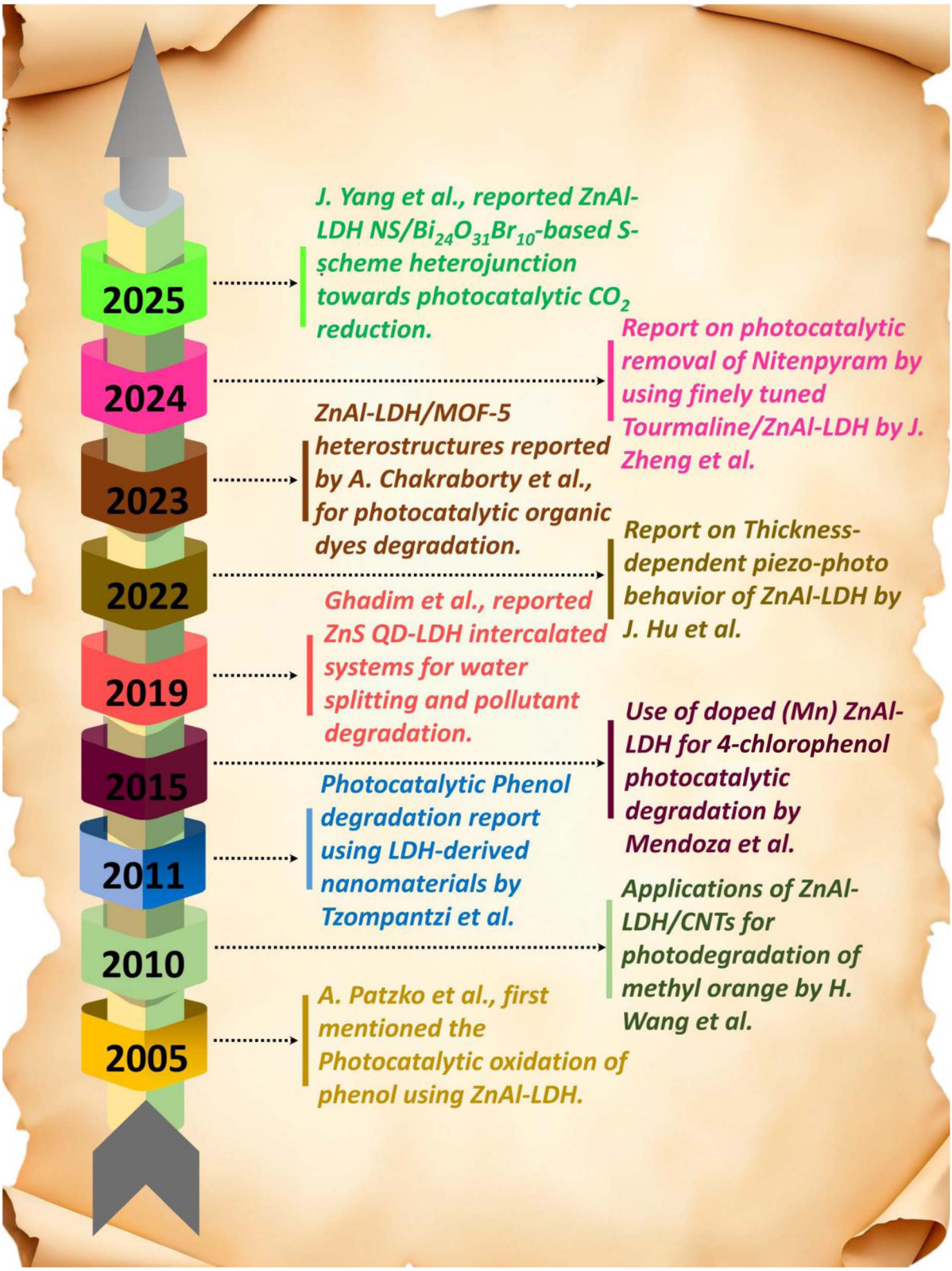

Scheme 1 A pictorial representation of growth trend for ZnAl-LDH and modified ZnAl-LDH towards photocatalytic and piezo-photocatalytic applications.

subjected to UV radiation due to its wider bandgap and the proportion of it in the material determines the photocatalytic capacity of ZnAl-LDH.[45,46]

2.2. Importance of Zn^{2+} in ZnAl-LDH

The presence of Zn^{2+} is also essential for achieving a superior phase in the layered structure of ZnAl-LDH. Further, the coordinatively unsaturated sub valent Zn^{2+} cations are produced by dispersing ZnO_6 octahedra in the LDHs lattice, which generates surface defects like O_Vs that act as electron trapping sites to capture photoelectrons, enhancing their outstanding performance in photocatalytic pollutant decomposition, oxygen evolution, and CO reduction. The inclusion of Zn^{2+} decreases interlayer distances in LDHs due to the larger electronegativity, and small crystallite size effectively inhibits photogenerated electron and hole recombination. The quantity of Zn directly correlates with the size of the crystal, resulting in a reduction in surface area. Consequently, the LDHs with a low Zn concentration will have a large surface area and low crystallinity, favouring excellent adsorption capacity toward reactant molecules facilitated by the broad distribution of macropores. Moreover, minimal thermal regeneration method and high anion retention capacity of ZnAl-LDH materials boost their photocatalytic performance.[47] Furthermore, DFT studies revealed the optimal lattice parameters and structure of ZnAl-LDH model based on prior publications as shown in Fig. 1a. The bare ZnAl-LDH has a $3 \times 3 \times 1$ supercell, (110) and (003) diffraction peaks with unit lattice variables of ($a = b = 3.08$ Å, $c = 7.75$ Å). The supercell has a 2 : 1 Zn : Al ratio, with one Al atom surrounded by six Zn atoms forming an octahedral structure and the Zn–O bond length of pristine ZnAl-LDH is 2.08 Å (Fig. 1b).[48]

3. Synthesis route and physicochemical characterization of ZnAl-LDH-based heterostructures

This section reviews several synthesis methods, including co-precipitation, hydrothermal, mechanochemical, electrostatic self-assembly, and others, used to create ZnAl-LDH-based composites. These techniques enable the development of modified ZnAl-LDH materials with specific physical and chemical features for various photocatalytic applications such as water splitting, pollutant degradation, and CO_2 reduction. Multiple characterization techniques like X-ray diffraction (XRD), high-resolution transmission electron microscopy (HRTEM) and field emission scanning electron microscopy (FESEM), BET (Brunauer–Emmett–Teller), FT-IR (Fourier-transform infrared) spectroscopy, thermogravimetric analysis (TGA), valence band X-ray photoelectron spectroscopy (VB-XPS), energy-dispersive X-ray spectroscopy (EDS) and atomic force microscopy (AFM) reveal the tailored chemical compositions, structures, optical, electronic, and chemical properties, as well as the morphologies of the photocatalysts that significantly influence their photocatalytic performance.[43,49] A schematic of the synthesis process and physico-chemical characterization techniques is presented in Scheme 2 alongwith the advantages and disadvantages overview of various synthesis techniques in Table 1.

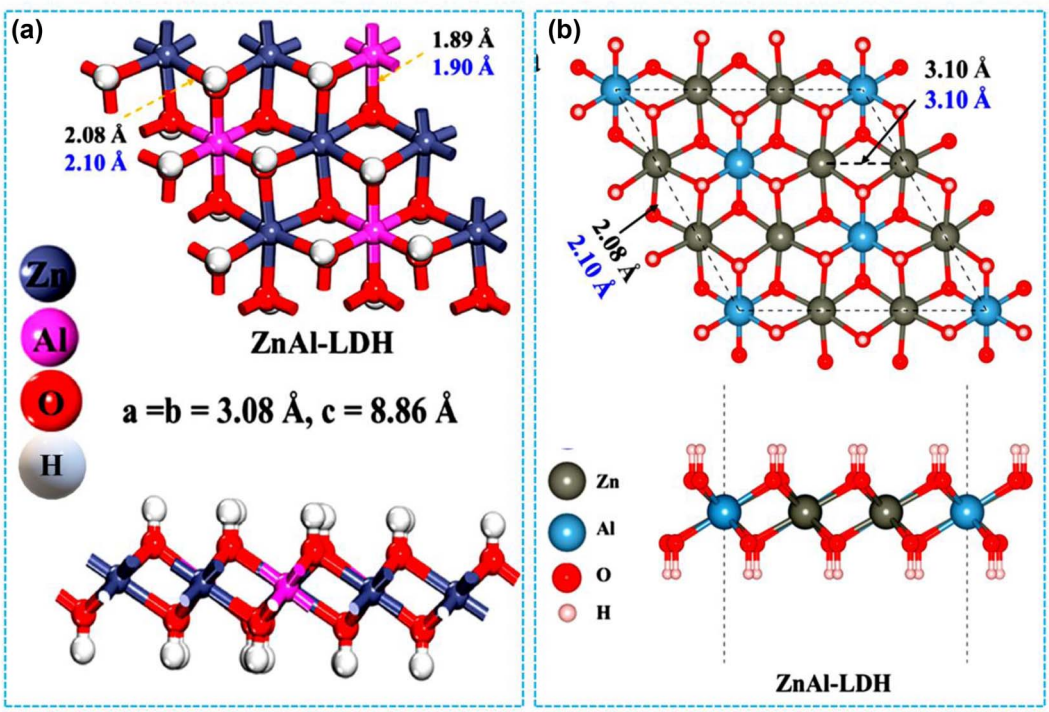

Fig. 1 (a) Structural model of ZnAl-LDH, (b) key geometrical parameters of three ZnAl-LDHs with DFT values in black and experimental values in blue, reproduced with permission from MDPI. Copyright © 2023.[48]

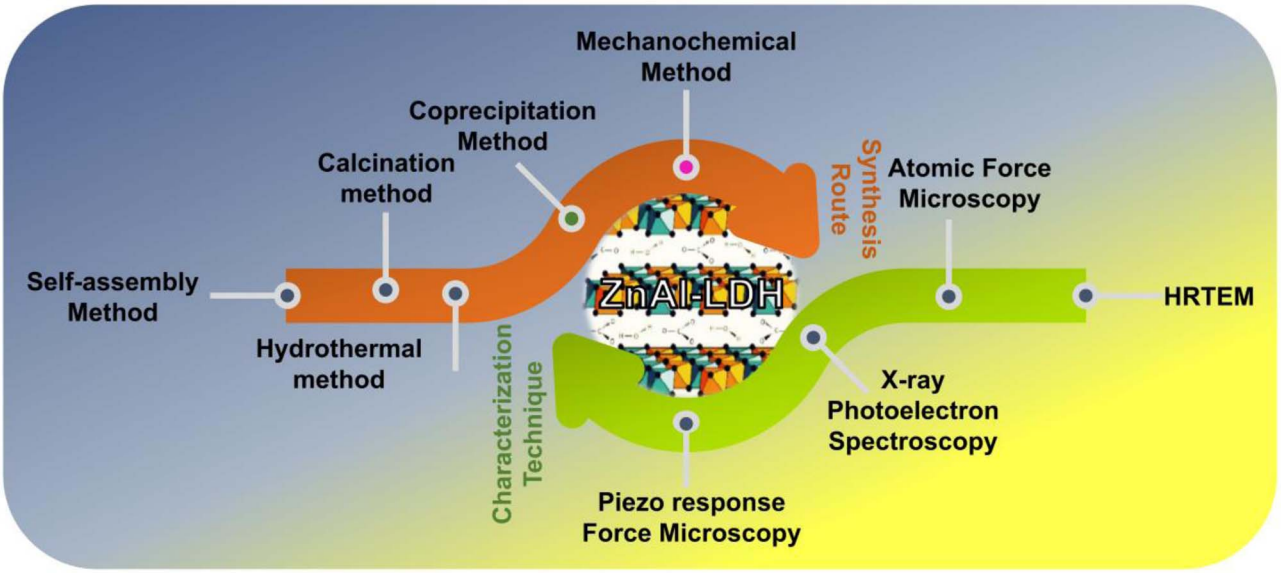

Scheme 2 Illustration of different synthesis procedures and various characterisation techniques involved in the preparation of ZnAl-LDH mediated systems.

3.1. Co-precipitation method

Co-precipitation is the most often used technique for making LDHs, which includes mixing solutions of trivalent and divalent metal salts in a specific ratio. The pH is increased by adding an alkaline solution and stirring vigorously; this causes LDHs made of two metal salts to co-precipitate. Aging the reaction mixture helps develop a consistent and well-crystallized LDHs structure. Both metal salts precipitate at the same time because the pH is kept relatively high. After filtering, the precipitate is washed with deionized water and dried in a furnace overnight. Carbonate ions from dissolved CO_2 in the environment might intercalate between hydroxide layers of LDHs, as carbonate ions are strongly bonded anions in the LDHs lattice. Therefore, reactions should be carried out in environments free of CO_2 or with N_2. This method can be used to create LDHs-based composites and pure LDHs.[2] The coprecipitation approach offers precise control of nanomaterial morphology by adjusting parameters like pH, temperature, concentration, and surfactant use.[50] In the pioneering work by Haiping Li *et al.* coprecipitation synthesis was used to create

Table 1 Overview of the advantages and disadvantages of various synthesis techniques

Synthesis techniques	Advantages	Disadvantages
Co-precipitation	• Easy procedure with regulated reaction conditions	• Strict pH control required
	• Excellent for producing uniform and fine nanoparticles with high yield and purity	• Undesired ions (*e.g.*, hydroxides, carbonates) may be introduced at high pH or in open-air environments
	• Scalable for industrial production	• Possible agglomeration of particles
Hydrothermal	• Precise control over temperature, crystallization timing, and interlayer composition	• High energy consumption when combined with other materials
	• Create LDH phases with larger particle sizes	• Requires specialized equipment and high reaction temperatures
Mechanochemical	• Faster, easier, and cleaner process than conventional synthesis methods	• The obtained product often has an amorphous (non-crystalline) structure
	• Enables access to previously unattainable molecular structures	• Competing reactions may produce unintended compounds
Calcination	• Allows controllable and adjustable composite structures	• High cost of the process
	• Enhances thermal stability of nanomaterials through high-temperature processing	• Susceptibility to contamination due to low-quality raw materials
	• Facilitates the removal of volatile substances	• Limited functional properties of the resulting materials
Electrostatic self-assembly	• Can produce a wide range of shapes	• Involves non-linear electric fields
	• Enables diverse functionalities	• Faces strict spatial charge constraints
	• Effective across multiple length scales	

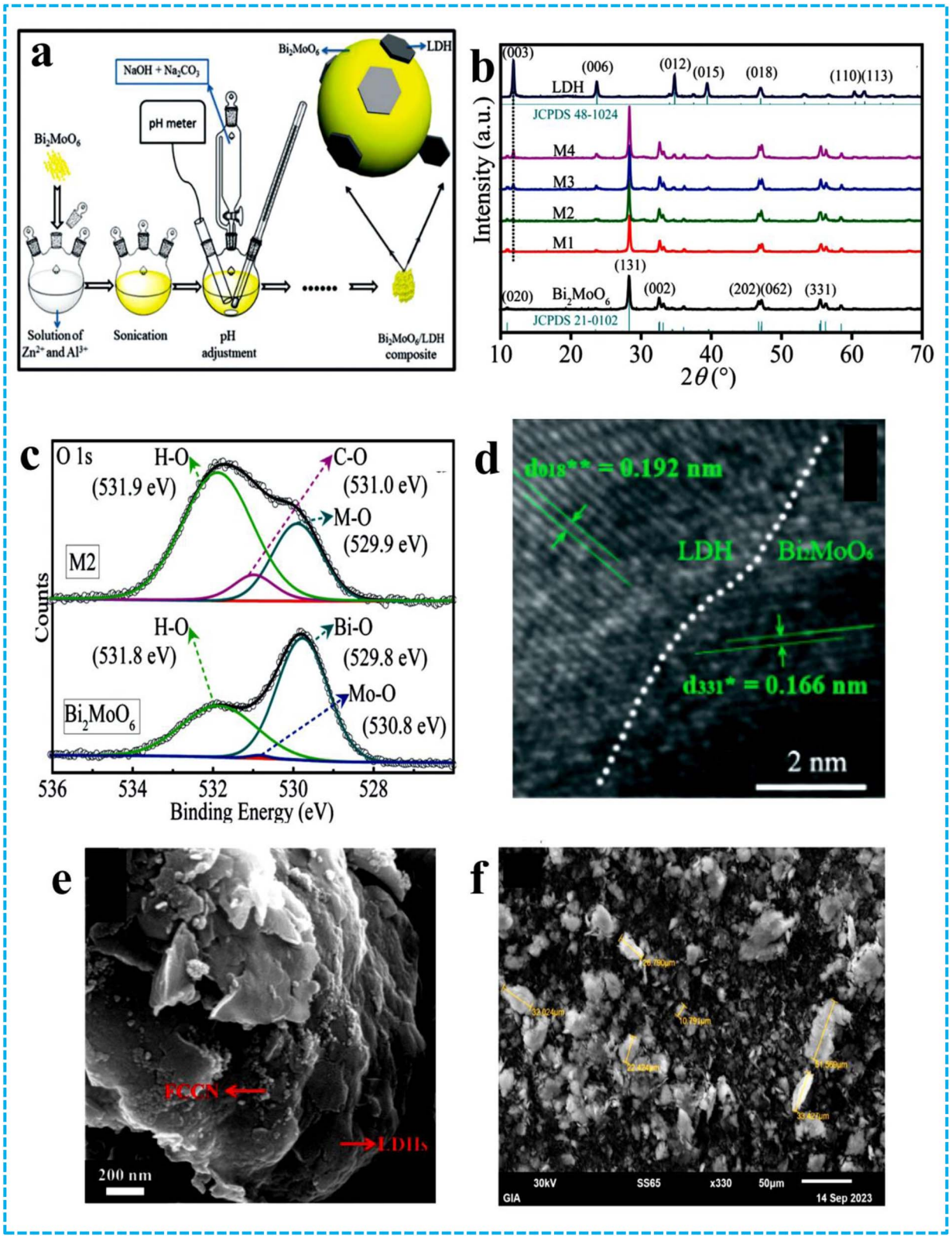

Fig. 2 (a) Schematic illustration of the synthesis of Bi_2MoO_6/ZnAl-LDH hybrid, (b) corresponding XRD patterns of neat and nanocomposites, (c) high-resolution XPS spectra of O 1s, (d) HRTEM image of M2, reproduced with permission from Royal Society of Chemistry. Copyright © 2023.[51] (e) SEM images of FCCN/LDH-100 hybrid, reproduced with permission from Elsevier. Copyright © 2023.[52] (f) FESEM image of 10% C_{60}-doped ZnAl-LDH/PVA reproduced with permission from Wiley. Copyright © 2024.[53]

Bi_2MoO_6/ZnAl-LDH composites. The composite was formed by combining ZnAl-LDH nanosheets with Bi_2MoO_6 hollow spheres (Fig. 2a). The successful formation of composite confirmed by XRD peaks revealed orthorhombic phase of Bi_2MoO_6 as depicted in Fig. 2b. XPS spectra (Fig. 2c) reveal increased Bi and Mo binding energies in the composite, indicating strong interfacial contact, suggesting electron transfer from Bi_2MoO_6 to ZnAl LDH through Zn (Al)–O–Bi, which provides additional (Mo) bonds and confirms the formation of a Bi_2MoO_6/ZnAl-LDH heterojunction. HRTEM pictures reveal that LDH nanosheets assembled onto Bi_2MoO_6 spheres (Fig. 2d) with two different sets of lattice fringes of 0.192 nm spacing matching to ZnAl-LDH(018) plane and 0.166 nm spacing corresponding to orthorhombic Bi_2MoO_6(331) plane.[51] In another study, J. Hu *et al.* fabricated a binary heterostructure of halogen F, Cl co-doped g-C_3N_4 on ZnAl-LDH (FCCN/LDH) *via* co-precipitation method. By the coprecipitation process, FCCN sheets were spread throughout the surface of LDH forming FCCN/LDH nanocomposite with a high electrostatic coupling of two 2D nanosheets (Fig. 2e). The hybrid exhibits the largest BET-specific surface area (70.13 $m^2\ g^{-1}$), average pore width (19.57 nm), and total pore volume (0.192 $cm^3\ g^{-1}$).[52] In addition, Balayeva and groups developed C_{60}-doped ZnAl-LDH/PVA composites by using the urea hydrolysis followed by coprecipitation methods.[53] The as prepared nanocomposite was formed by noncovalently doped and physically intercalation of C_{60} into the ZnAl-LDH/PVA composite, facilitated by the polymer support, which widen the basal spacing of ZnAl-LDH to 9.217 Å. The material demonstrates a characteristic ZnO rice-shaped 2D morphology (100 nm to 2 μm broad, 500 nm to 10 μm long, Fig. 2f). Several composites and heterojunctions combining with ZnAl-LDH have been effectively fabricated using the co-precipitation process, with each presenting a distinct morphology that can be compared through there FESEM images as illustrated in the below FESEM images.

3.2. Hydrothermal method

The hydrothermal or solvothermal methods are a technique assisted by temperature- and pressure that produces nanostructured materials. This entails a heterogeneous chemical reaction by inserting a mixture of metal salts and a precipitating agent into a sealed Teflon coated autoclave and then treating it at high temperatures (100 °C) and pressures (1 bar). The technique is broadly suited to the synthesis of materials with a variety of morphologies, including nanosheets, nanoflowers, nanospheres, nanorods, and nanowires, as well as their clusters with tuneable structural complexity, size, shape, and phase. The hydrothermal approach is advantageous for synthesizing minerals, since it can preserve high crystallinity, avoid accumulation, and yield higher-purity samples.[2] In this context, Lin Wang and his research groups designed Bi-doped ZnAl-LDH (BZA) augmented with O_Vs by the hydrothermal synthesis method as shown in Fig. 3a. They investigated various characterisation techniques to illustrate the influence of Bi^{3+} doping into ZnAl-LDH on the energy band structure and formation of O_Vs. Since Bi atoms have a bigger radius and a higher ionization potential than Al atoms, they are more likely to form Bi–O links, which quickly cause lattice deformation and the production of

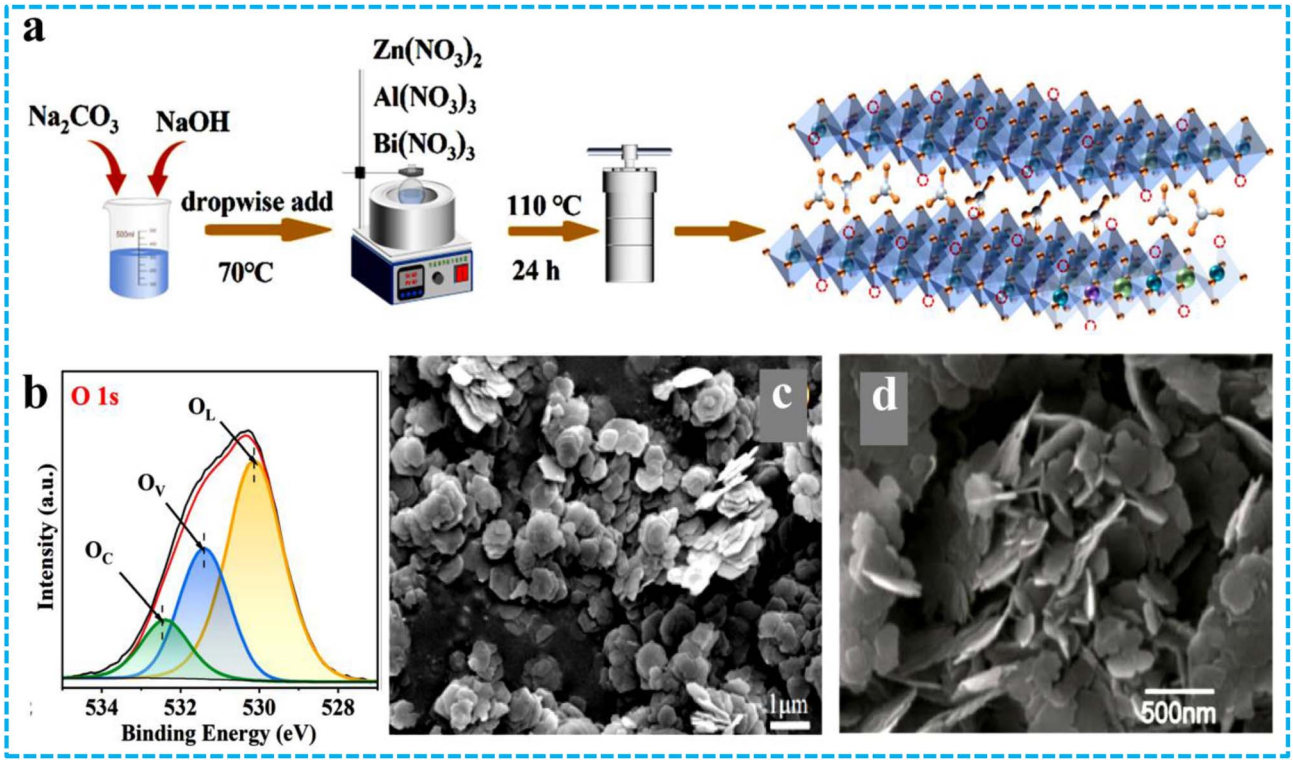

Fig. 3 (a) Schematic illustration of preparation processes of BZA-*X*, (b) XPS spectra of O 1s in BZA-0.5, reproduced with permission from Royal Society of Chemistry. Copyright © 2024.[54] FESEM image of (c) Zn–Al LDHs, reproduced with permission from Elsevier. Copyright © 2022.[55] (d) MoS_2/LDH, reproduced with permission from Elsevier. Copyright © 2020.[56]

O_Vs. The increasing Bi doping ratio led to a steady decrease in the distinctive diffraction peaks, and a shift towards higher angles was observed. This indicates that the addition of Bi^{3+} effortlessly induces lattice deformation to develop O_Vs and a decrease in crystallinity due to the replacement of Al^{3+} (0.51 Å) by Bi^{3+} (1.2 Å) species with a higher atomic radius in ZnAl-LDH. The HRTEM data validate the ortho-hexagonal structure of the material with lattice stripes and 0.22 nm stripe spacing corresponding to the (015) surface of ZnAl-LDH. Local disorder and disruption in the material lattice strips confirmed that the atomic defects on the surface of the material with deformed scratches resulted from the creation of an O_V. Further, according to Electronic Paramagnetic Resonance (EPR) and XPS data, BZA has the highest concentration of surface O_Vs and the strongest signal strength, suggesting that the doping of Bi^{3+} supports the creation of O_Vs on the material's surface. Again, Bi doping enlarged the lattice (Fig. 3b), which leads to dislocation and local disorder along with the dispersion of oxygen atoms on the surface, that creates O_Vs.[54]

In another attempt, M. Wang and his groups created In_2S_3/ZnAl-LDH composites by employing a single-pot hydrothermal method taking $InCl_3$ and TAA as precursors. In the course of the one-pot hydrothermal process, the In_2S_3 nanoparticles nucleate and grow on LDHs surface detailed in FESEM images (Fig. 3c). The two components establish a heterojunction interface because the In_2S_3 nanoparticles are well-dispersed and anchored onto ZnAl-LDH nanosheets, and LDHs serve as a scaffold to stabilize In_2S_3.[55] Similarly, S. Chen *et al.* prepared MoS_2/ZnAl-LDH heterojunctions using coprecipitation and hydrothermal methods to modulate band gap engineering. Using the hydrothermal method, MoS_2 appears as tiny globules ranging from 100 to 150 nm, while ZnAl-LDH forms large, layered structures measuring between 10 and 20 μm through coprecipitation. In the MoS_2/LDH composite (Fig. 3d), the LDH layers resemble leaves, whereas MoS_2 is evenly distributed as single layers or points on the hydrotalcite surface.[56] Based on the hydrothermal method, numerous ZnAl-LDH-based nanomaterials with various modifications have been successfully synthesized, each exhibiting a distinct morphology every single time relevant with the corresponding FESEM images shown in the below figures cited from different literatures.

3.3. Mechanochemical method

The repetitive welding, deformation, and fracture of the reactant combination is known as mechanochemical processing. The process of creating materials through mechanochemical construction involves introducing the solid-state system with a significant amount of strain and defects. This causes the raw material particles to deform violently and creates internal vacancies and alterations, which in turn promote the dispersion of atoms or ions. Simultaneously, the ongoing collisions among the particles will consistently create new surfaces, reduce the dispersion distance, and promote chemical reactions.[57] T. Ma *et al.* mechanochemically constructed Bi_2WO_6/ZnAl-LDH heterojunction as illustrated in Fig. 4a. The uniform distribution of Bi_2WO_6 particles on the LDH matrix, which forms a well-structured heterojunction by a mechanochemical method, is confirmed by SEM (Fig. 4b). Mechanical energy facilitates the close contact and interfacial bonding between Bi_2WO_6 and LDH. This creates a heterostructure interface that permits mutual stability and electronic interaction. The nanohybrid indicates a flocculated morphology of LDH structure with irregularly shaped Bi_2WO_6 particles evenly distributed over its surface emphasizing the efficiency of the mechanochemical process in creating homogenous composites. It is clearly evident from Fig. 4c that the individual reflections corresponding to the Bi_2WO_6 and LDH can also be identified in the Bi_2WO_6/ZnAl-LDH heterojunction samples. XPS analysis further confirms the formation of heterojunction as shifting in Zn 2p (Fig. 4d) and Bi 4f (Fig. 4e) binding energies reveals strong chemical interactions between ZnAl-LDH and Bi_2WO_6 instead of physical mixing because of mechanochemical synthesis.[58] Furthermore, Z. Li group designed an innovative Z-scheme heterostructure of Bi_2S_3/ZnAl-LDH photocatalyst by mechanochemical synthesis. The effective creation of Bi_2S_3/ZnAl-LDH nanocomposites was verified by XRD analysis, which displayed distinctive peaks of orthorhombic Bi_2S_3. Bi_2S_3 nanoparticles were effectively incorporated into the ZnAl-LDH matrix during milling. In the Bi_2S_3/LDH sample, the primary diffraction peaks of pure Bi_2S_3 and LDH had changed intensity, suggesting that one component affected the formation and reorientation of other crystal throughout the mechanochemical process.[59] Lately, Li and co-authors showcased the insertion of Pt co-catalyst into ZnAl-LDH nanoparticles by the mechanochemical approach to stimulate the chemical bonds in the primary zinc carbonate and aluminium hydroxide structure, resulting in the synthesis of LDH. Due to a large ionic radius and exceptionally high chemical stability, Pt couldn't substitute Zn or Al in the LDH lattice; instead, it can only be inserted in its elemental state into the LDH matrix. A tight heterojunction is established at the biphasic combination between Pt and LDH as metallic Pt nanoparticles are disseminated evenly around the exterior surface of the LDH matrix.[60]

3.4. Calcination method

Calcination is a process of applying heat to a solid chemical compound to eliminate impurities or volatile substances and cause thermal decomposition. The compound is heated to an elevated temperature without melting while being supplied with a minimal amount of ambient oxygen (the gaseous O_2 fraction of air). LDHs transformed to MMOs at 450–500 °C, which have a large surface area and an appropriate dispersion of metal cations. The memory effect that MMOs display enables them to mimic their layered morphology through the absorption of anions, by utilizing all successive layers of MMO that have numerous reactive centres after calcination. The large specific surface area of MMO effectively resists photo corrosion while conversion into MMO enhances the multifunctionality of LDH-based photocatalyst by enhancing structure crystallinity, electron mobility, reducing layer aggregation.[20] In light of this, D. A. Islam *et al.* designed ZnAl-LDH derived ZnO nanorod on etched graphene oxide (GO) nanosheet by the calcination method and

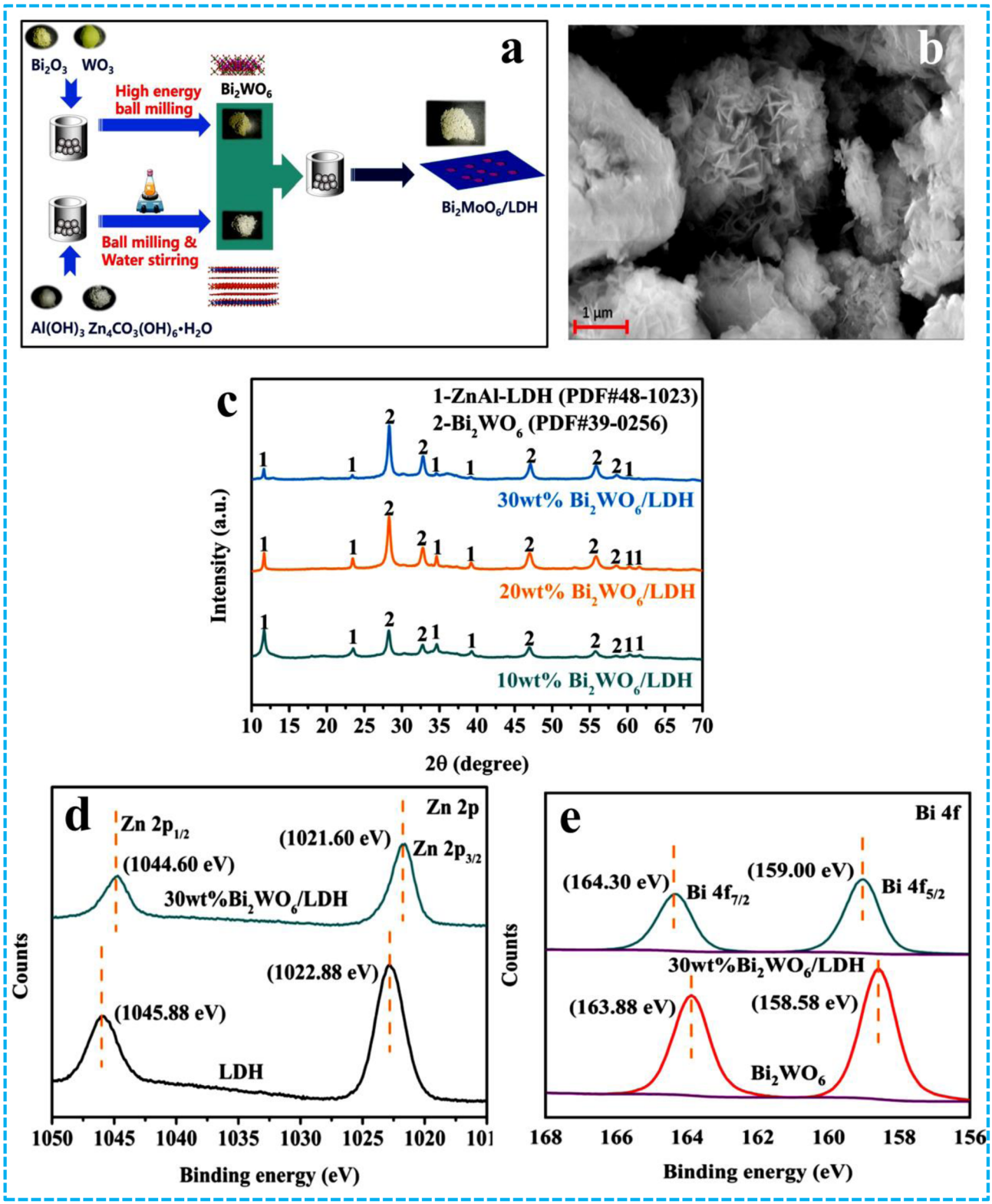

Fig. 4 (a) Mechanochemical procedure and corresponding structures for Bi_2WO_6, LDH, and Bi_2WO_6/LDH heterojunctions, (b) corresponding SEM image of 30 wt% Bi_2WO_6/LDH, (c) XRD patterns for as-synthesized Bi_2WO_6/LDH samples with various wt% Bi_2WO_6 dosages, XPS spectra for (d) Zn 2p, (e) Bi 4f for the LDH, Bi_2WO_6 and 30 wt% Bi_2WO_6/LDH samples, reproduced with permission from Elsevier. Copyright © 2021.[58]

subsequently by *in situ* development of the LDH on the GO nanosheets. As evident in Fig. 5a *via* an *in situ* co-precipitation method, the ZnAl-LDH/GO nanocomposite was produced first. Then a facile wet chemical decomposition approach was utilized to develop LDH generated ZnO nanorods deposited GO nanocomposites in an alkaline environment. Highly distributed ZnO

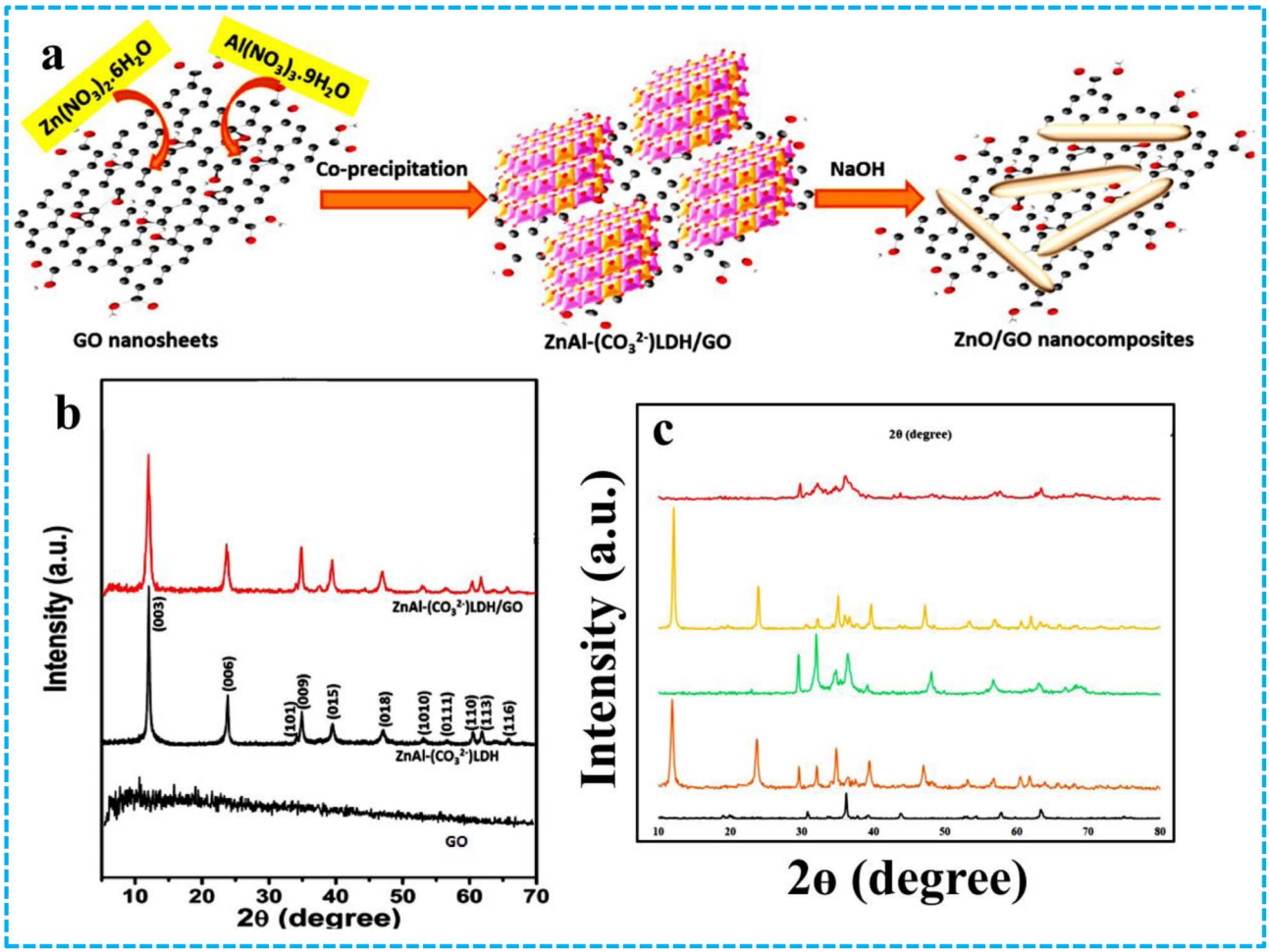

Fig. 5 (a) Fabrication procedure of ZnO/GO nanocomposites, (b) PXRD profile of ZnAl-(CO_3^{2-})LDH, ZnAl-(CO_3^{2-})LDH/GO, reproduced with permission from Elsevier. Copyright © 2024.[61] (c) XRD pattern for $NiFe_2O_4$, Zn–Al LDH, MMO, $NiFe_2O_4$–Zn–Al LDH, $NiFe_2O_4$–MMO, reproduced with permission from Elsevier. Copyright © 2021.[62]

nanorods on GO nanosheets were created by the thermochemical breakdown of the ZnAl-LDH/GO composite at 80 °C. The powder XRD (PXRD) pattern of the ZnAl-(CO_3^{2-}) LDH/GO composite closely matches that of pristine ZnAl-(CO_3^{2-}) LDH, indicating that the LDH crystalline phase is preserved upon incorporation of GO (Fig. 5b). The increased surface area of graphene oxide (GO) facilitates the creation of evenly dispersed ZnO nanorods with regulated size and the improved photocatalytic performance may be achieved by tuning the band gap of ZnO nanorods by altering the GO concentration. The TGA arc of ZnAl-(CO_3^{2-}) LDH/GO determined early loss of weight at 100 °C owing to the desorption of free carbon dioxide and H_2O followed by at 280 °C due to intercalated CO_3^{2-} and H_2O removal, and due to layered structure disintegration. A higher overall weight reduction in the ZnO/GO nanocomposite indicates the presence of GO in the composite. ZnO/GO nanocomposites possess a uniform distribution and a smooth surface of ZnO nanorods with the spherical development and aggregation of 10–15 nm-diameter ZnO nanoparticles. The formation of homogeneous ZnO nanorods with hexagonal crystalline wurtzite is regulated by the GO surface as the GO layers serve as a platform for the nucleation and orientational growth of ZnO nanorods, thereby averting their accumulation. The lattice fringes between two neighbouring planes of a ZnO nanorod are approximately 0.26 nm, which resembles to the (002) plane of the wurtzite hexagonal morphology of the ZnO nanorod. The study of morphology emphasizes the importance of GO in regulating the size, shape, distribution, and crystallinity of ZnO nanostructures by calcination.[61] Furthermore, P. Veisi and groups prepared $NiFe_2O_4$/ZnAl-LDH MMO composite and they studied the integrated effect of photocatalysis and adsorption in removing organic pollutants from contaminated water. The primary processes that drive the $NiFe_2O_4$/ZnAl-LDH and its calcined counterpart ($NiFe_2O_4$–MMO) are hydrothermal synthesis and calcination, which result in structural integration and transformation. In composite, $NiFe_2O_4$ particles embedded in a matrix of mixed metal oxides, increasing visible light activity, electrical conductivity, and surface area. The diffraction pattern of the nanocomposite demonstrates the absorption peaks associated with MMO, ZnAl-LDH, and the $NiFe_2O_4$ spinel structure. A variety of metal oxides, including ZnO crystal composition in the hexagonal phase, $Zn_6Al_2O_9$ in the cubic phase and $ZnAl_2O_4$ spinel structure in the FCC cubic phase, were also represented by the peaks revealed the effective synthesis of $NiFe_2O_4$–MMO heterostructure as shown in Fig. 5c. The destruction of interlayer bonds

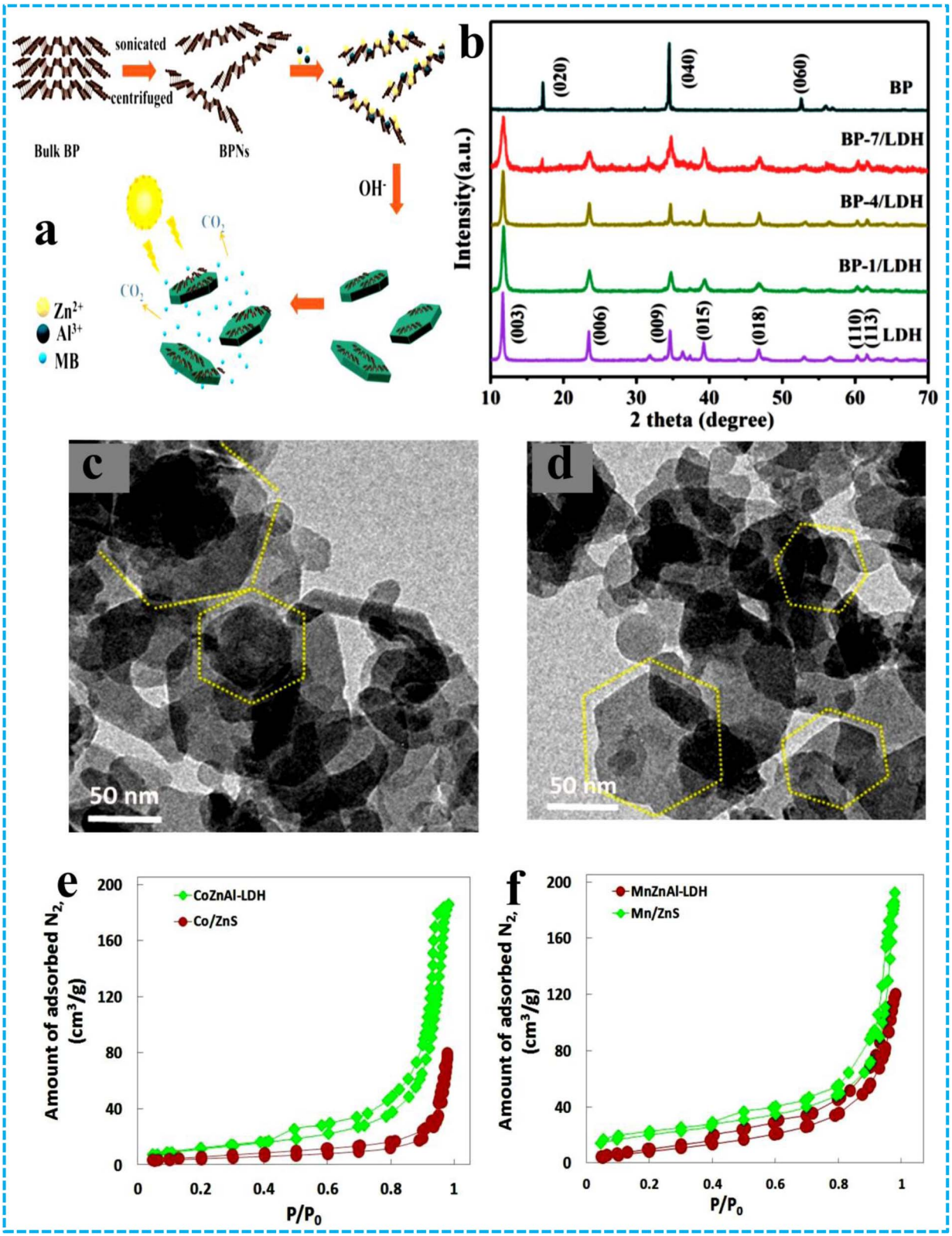

Fig. 6 (a) Fabrication process of BP/LDH, (b) XRD patterns of BP, ZnAl-LDH, BP-1/LDH, BP-4/LDH, and BP-7/LDH, reproduced with permission from Elsevier. Copyright © 2021.[64] Low-magnified TEM images of (c) CoZnAl-LDH, (d) MnZnAl-LDH. N_2 adsorption/desorption isotherms of (e) CoZnAl-LDH and Co/ZnS samples, and (f) MnZnAl-LDH, and Mn/ZnS samples, reproduced with permission from Royal Society of Chemistry. Copyright © 2019.[37]

during calcination causes ZnAl-LDH to change into MMO (ZnO, $Zn_6Al_2O_9$, $ZnAl_2O_4$), which has a larger thickness (50–80 nm). In the $NiFe_2O_4$/ZnAl-LDH composite, $NiFe_2O_4$ crystals were observed on LDH plates and in the $NiFe_2O_4$–MMO composite, $NiFe_2O_4$ was inserted in the calcined mixed oxide matrix.[62]

3.5. Electrostatic self-assembly method

A spontaneous process termed as self-assembly allows disorganized structural components or nanostructures in the desired arrangement using electrostatic forces. Employing the attraction between species with opposing charges, this technique constructs layers or structures in a controlled way. Because of its unique nano-architectonics and tunable chemical composition, the layer-by-layer (LBL) self-assembly technology offers a flexible approach to constructing precise multi-layer nanohybrids.[63] In this example, J. Yang and team designed ZnAl-LDH@BP nanocomposite influenced by the electrostatic interaction as illustrated in (Fig. 6a). The BPNs were produced using liquid exfoliation, and interact with ZnAl-LDH through electrostatic self-assembly due to their opposing zeta potentials (−12.2 mV for BPNs and +42.8 mV for LDH). In the BP/LDH composites, decreased and broadened LDH peak intensity were observed, indicating reduced crystallinity and smaller particle size because of higher and successful incorporation of BPN content revealed in Fig. 6b. ZnAl-LDH showed regular, hexagonal flaky platelets but the introduction of BPNs increased dispersity and decreased platelet size, resulting a rough surface. As a result of the electrostatic attraction, contact between BPNs and ZnAl-LDH, size of ZnAl-LDH decreased with preventing aggregation.[64]

In another attempt, A. R. Amani-Ghadim and his research groups synthesized heterostructure *via* self-assembling of oppositely charged binary ZnAl-LDH/ZnS QDs and ternary MIIZnAl (MII = Ni, Co, and Mn) LDHs/ZnS QDs using 3-mercaptopropionic acid (MPA) as capping agent. In this nanocomposite ZnS QDs were partially introduced within the interlayer's region of LDHs. The ZnS QDs/LDH composite using self-assembly synthesis method successfully alters the CoZnAl-LDH and MnZnAl-LDH morphology, produces more compact nanosheet assemblies, enhanced particle dispersion, and intercalated structures with enlarged layers speculate by TEM data in Fig. 6c and d. As illustrated in Fig. 6e and f, Mn/ZnS has a smaller surface area whereas Co/ZnS has a greater surface area than pristine LDH. The reduction in surface area was caused by partial intercalation of particles in the interlayer space of LDH and ZnS quantum dots being deposited on the exterior planar surface.[37]

4. Fundamental insights into the underlying mechanisms of the various photocatalytic applications

The mechanism of photocatalysis involves the light-absorption potential of a semiconducting material to generate electron–hole pairs that drive redox reactions at the material's surface. As a result, photocatalysis serves the major concerns relating environmental remediation and energy generation. In other words, photocatalysis aims to mimic the natural photosynthetic pathway by converting solar energy into chemical fuels (*e.g.*, H_2 or hydrocarbons) from water and/or carbon dioxide under controlled conditions. A key advantage of photocatalysis is its relative simplicity and applicability that can leverage more complex reaction pathways and higher value chemical outputs under ambient conditions, but it typically demands more precise material design, tighter band-edge alignment, and often suffers from lower stability and scalability. When a semiconductor photocatalyst is irradiated with light of energy equal to or greater than its band gap, electrons in the valence band (VB) are excited to the conduction band (CB), leaving behind an equivalent number of holes in the VB. This leads to the generation of electron–hole pairs, which are the fundamental reactive species responsible for driving chemical transformations. The mechanism typically proceeds through four sequential steps: (i) light absorption: the photocatalyst absorbs photons with energy greater than or equal to band gap. (ii) Charge generation: electron–hole pairs are created within the semiconductor lattice. (iii) Charge migration and separation: electrons and holes migrate to the surface *via* diffusion or internal electric fields, ideally remaining separated. (iv) Surface redox reactions: electrons reduce species such as O_2 or H^+, while holes oxidize water, hydroxide ions, or organic molecules. The photoexcited electrons in the conduction band possess sufficient reduction potential to react with electron acceptors, such as molecular oxygen, forming ROS like superoxide radicals ($O_2^{\bullet -}$). Simultaneously, the holes in the valence band act as strong oxidizing agents and can oxidize water or hydroxide ions to produce hydroxyl radicals ($^{\bullet}OH$). These ROS are highly reactive intermediates capable of decomposing organic pollutants, reducing CO_2, or splitting water into H_2 and O_2. However, the overall photocatalytic efficiency of a semiconductor strongly depends on the competition between charge separation and recombination. Rapid recombination of photoinduced electron–hole pairs dissipate energy as heat or light, reducing the number of carriers available for surface reactions. Therefore, strategies such as heterojunction formation, metal or non-metal doping, cocatalyst loading, and surface modification are employed to promote charge separation, suppress recombination, and extend light absorption into the visible region.[65]

4.1. Photocatalytic hydrogen evolution reaction (HER)

Photocatalytic water splitting is a potential technique for splitting water into H_2 and O_2, helping to address environmental and energy issues. The process is endothermic, thermodynamically uphill with change in standard Gibbs free energy (ΔG°) 237 kJ mol^{-1}, and requires external energy input. The detailed processes are shown in Scheme 3. Thermodynamic studies indicate that water electrolysis becomes possible when the CB potential of the semiconductor is more negative than H^+/H_2 (0 V *vs.* NHE) and more positive than O_2/H_2O (1.23 V *vs.* NHE). Upon light irradiation, the photogenerated excitons produced are separated and migrated towards the VB and CB of LDHs, followed by migration to the surface of the photocatalyst (Scheme 3a). The photoexcited electrons combine with H^+ to form hydrogen, while the holes oxidize water to produce O_2.[49] Throughout the water

splitting process, photo-oxidation and photo-reduction reactions occur simultaneously at the VB and CB, respectively.[28] The excited electrons participate in a reduction reaction with protons to produce hydrogen, while sacrificial reagents or water consume the holes to generate protons and O_2. Redox activity can be enhanced by using sacrificial agents such as ethanol, glycerol, lactic acid, triethanolamine (TEOA), and methyl. This is because each photocatalyst interacts differently and exhibits varying efficiencies with these sacrificial agents due to their different adsorption abilities and available protons.

$$H_2O + 2h^+ \rightarrow 2H^+ + 1/2O_2 \quad E^\circ = +1.23\ V \tag{1}$$

$$2H^+ + 2e^{-1} \rightarrow H_2 \quad E^\circ = 0.00\ V \tag{2}$$

$$H_2O \rightarrow H_2 + 1/2O_2 \quad \Delta E^\circ = 1.23\ V\ (\Delta G^\circ = 278\ kJ\ mol^{-1}) \tag{3}$$

Photocatalytic water splitting using semiconductor-based photocatalysts effectively uses the solar energy to split H_2O molecules into H_2 and O_2. This overall water dissociation is a multielectron, energetically uphill and endothermic process with a huge positive change in Gibbs' free energy (ΔG° = +238 kJ mol^{-1}; 2.46 eV per molecule). For reduction to happen, the semiconductor's CB edge potential needs to be (H^+/H_2 = 0.00 V *vs.* NHE at pH = 0 or −0.41 V *vs.* at pH = 7) and the VB edge must be greater than the water's oxidation potential (O_2/H_2O = +1.23 V *vs.* NHE at pH = 0 or +0.82 V *vs.* NHE at pH = 7) to perform overall water splitting. Hence, a requisite bandgap energy of 1.23 eV is required to complete the water-splitting process effectively.[20]

4.2. Photocatalytic pollutant degradation

Eco-friendly methods for destroying industrial wastewater pollutants like phenol, dye, petroleum hydrocarbons, and

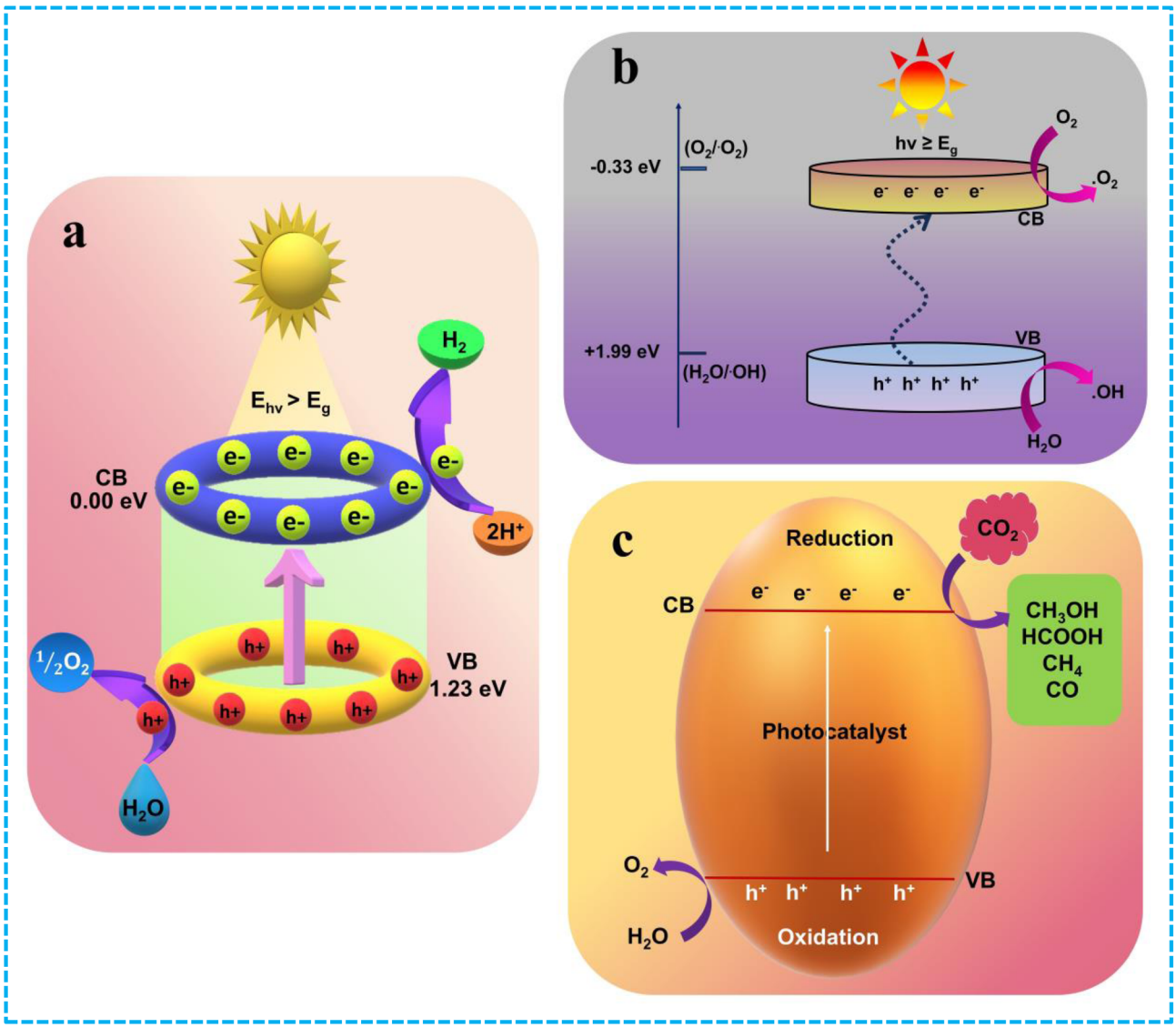

Scheme 3 (a) Schematic representation of HER, (b) schematic illustration of photocatalytic pollutant degradation, and (c) schematic visualization of photocatalytic CO_2 reduction.

antibiotics are becoming an urgent concern owing to their detrimental impacts on aquatic life and their possible carcinogenic hazards pose to people. Among them, photocatalytic degradation is an emerging approach that transform harmful environmental pollutants into less toxic materials on a semiconductor photocatalyst (Scheme 3b). The intricate mechanism of photocatalytic pollutant degradation is elucidated in the following reactions.[21,66]

$$\text{Photocatalyst} + h\nu \rightarrow e^- + h^+ \quad (4)$$

$$O_2 + e^- \rightarrow O_2^{\cdot -} \quad (5)$$

$$O_2^{\cdot -} + H_2O \rightarrow HO_2^{\cdot} \quad (6)$$

$$H_2O/OH^- + h^+ \rightarrow {}^{\cdot}OH \quad (7)$$

$$O_2^{\cdot -}/HO_2^{\cdot}/{}^{\cdot}OH + OPs \rightarrow CO_2 + H_2O \quad (8)$$

4.3. Photocatalytic CO_2 reduction

One of the most prevalent gases in nature is CO_2, however in recent years, excessive CO_2 emissions have led to a variety of significant energy and environmental issues. Through photocatalysis, efforts have been made to transform CO_2 into useful compounds like C1 and C2 species. However, a π-bond between the p-orbital electrons on the carbon and oxygen atoms forms the stable linear molecule structure of CO_2. This means that reducing CO_2 requires a significant amount of energy, which creates high energy demands. The problem of excessive energy consumption in CO_2 valuable conversion is expected to be resolved by the suggested energy-free photocatalytic technique.[49] Since CO_2 is a highly stable ($\Delta G^\circ = -400$ kJ mol^{-1}) and inert molecule with linear configuration, it takes an immense amount of energy to break the C=O bond (750 kJ mol^{-1}) and create new C–H bonds during catalytic reduction process. The molecule is rendered inactive due to the large energy difference between the LUMO and the HOMO (13.7 eV) as well as the strong electron affinity of CO_2. Photocatalysis is a facile method for triggering and converting CO_2 into high-value-added chemicals including CO, CH_3OH, HCOOH, CH_4, and so on. Under solar light illumination, holes from the VB are usually engaged in some water oxidation, while e^- from the CB can contribute to the reduction of CO_2 (Scheme 3c). The distribution of the end products can vary depending on the type of reductant, operating conditions, and the quantity and potential of the charge carriers involved in the chemical reaction.[43,67]

$$CO_2 + 2e^- + 2H^+ \rightarrow HCOOH \quad (9)$$

$$CO_2 + 2e^- + 2H^+ \rightarrow CO + H_2O \quad (10)$$

$$CO_2 + 4e^- + 4H^+ \rightarrow HCHO + H_2O \quad (11)$$

$$CO_2 + 6e^- + 6H^+ \rightarrow CH_3OH + H_2O \quad (12)$$

$$CO_2 + 8e^- + 8H^+ \rightarrow CH_4 + 2H_2O \quad (13)$$

4.4. Conceptual interpretations of piezo potential enhanced photocatalytic mechanism

The rapid recombination of photogenerated charge pairs and the ineffective interfacial redox reaction generally lower the quantum efficacy and significantly restrict the photocatalytic performances. These limits of photocatalysis prompted the development of a new field of study called piezo-phototronics phenomenon, which combines the study of semiconductor physics, and their photo excitation process with piezoelectric science to exploit the piezoelectric polarization to change the initiation, separation, and migration of carrier charge pairs as well as recombination at the intersection and the peripheral surface is the fundamental idea of this process.[38,68] Therefore, a piezoelectric polarized photocatalysis is a sustainable methodology that incorporates both photocatalysis and piezo catalysis, where photocatalysis involves a light source conjunction with a semiconductor to induce the formation of charge carriers and their separation. In contrast, piezo catalysis relies on mechanical strain to excite and separate charge carriers. The synergistic integration of these two processes significantly enhances charge separation, thereby improving overall photocatalytic efficiency. Generally, piezo-photocatalysis is governed by the piezoelectric potential stimulated photocatalysis, which determines the potential of materials to accumulate solar energy, along with mechanical energy, or vibrational energy. The mechanism of piezo-photocatalysis entails two steps: first, photons with suitable energy stimulate electrons from the VB to CB; second, mechanical energy generates an internal electric field that restricts charge recombination and makes more feasible for photoelectrons to diffuse from the bulk to the surface initiating the reduction reaction. The accumulation of charges at the interface generates free radicals that react with the adsorbed molecules.[69,70] As mechanical strain is applied, there is a noticeable displacement in both occupied and unoccupied energy levels. The highest occupied molecular orbital (HOMO) and lowest unoccupied molecular orbital (LUMO) effects are only observable in piezocatalytic solutions, where the applied mechanical stress causes a piezo-potential, which bends the conduction band below the HOMO levels and allows charge carriers to migrate from the HOMO to the conduction band. On the other hand, electrons shift from the valence band to the LUMO that illustrated in Fig. 7. The combination of piezoelectric materials in photocatalysis aids in the execution of promising charge separation rather than utilizing numerous techniques like band gap tuning, anion doping, composite semiconductor formation, and defects formation, among others, for an efficient charge separation in a photocatalytic system.[71] Typically, non-centrosymmetric catalysts can undergo deformation and exhibit piezoelectric effects when exposed to external forces like ultrasonic waves, thermal stress, ultrasonication, stress and water flow, *etc.* These piezoelectric fields could prudently facilitate catalytic performance by contributing in the movement of induced charge carriers in bulk and surface of the photoactive material, which encourages separation and reduced the charge recombination and modifies the band structure at the heterogeneous interface.[72]

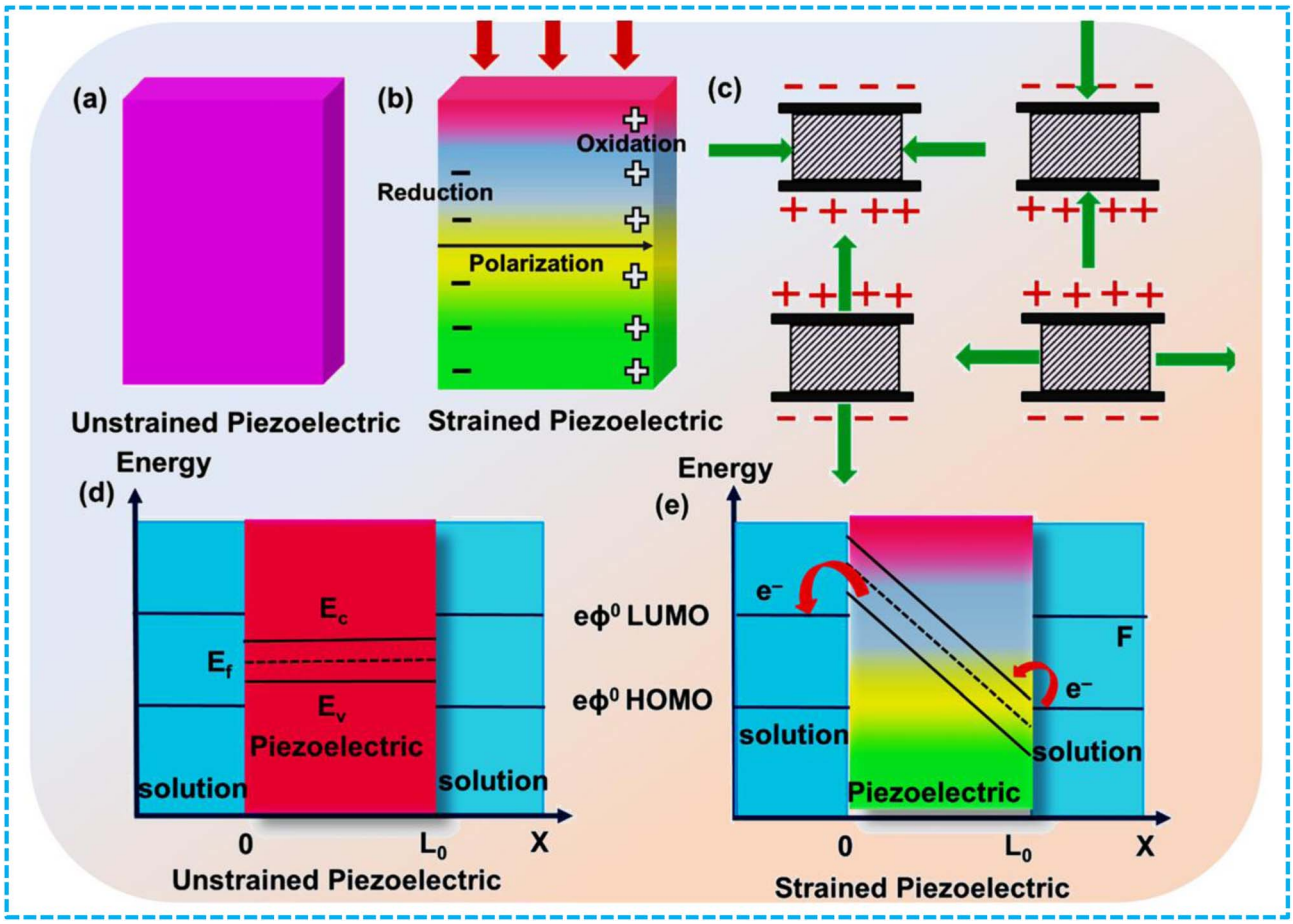

Fig. 7 (a–c) Diagrammatic representation of the piezo potential distribution subjected to external force, (d and e) band alignment under unstrained and strained environment, reproduced with permission from American Chemical Society. Copyright © 2024.[70]

5. Design strategies of the ZnAl-LDH-based high-performance catalysts towards various applications

ZnAl-LDH have strong tunability, which enables them to modify their architectural and electronic structures, implementing a variety of modification techniques to improve photocatalytic performance.[45] The development of ZnAl-LDH-based high-performance catalysts for exceptional activity and stability can be primarily patterned following structural and compositional variation for more active site exposure and structural adjustability by adopting various approaches such as (i) doping or defect engineering, (ii) heterostructure or composites formation, (iii) structural transformation *via* calcination and, (iv) interlayer anion adjustment, *etc.* This section provides insights into the developmental strategies for modification of ZnAl-LDH-based high-performance catalysts for different applications such as H_2 evolution, elimination of environmental contaminants, and CO_2 reduction *etc.* Table 2 reads the comparative analysis of the various modification strategies with respect to the advantages and disadvantages.

5.1. Doping or defect engineered ZnAl-LDH towards photocatalytic applications

Doping is an advanced technique that can significantly enhance light absorption and concurrently create beneficial defects in the LDHs structure for photoinduced carrier charge transfer ability. Doping also implies the inclusion of foreign metal cations into the LDH structure, which stimulates the basal plane to expose active sites, tunes its band gap, thereby enhancing its electron mobility. The photocatalytic performance of LDHs can be altered by incorporating a trivalent or tetravalent cation, often termed as "dopant" of the LDHs, in which trivalent or tetravalent is used alongside a bivalent cation. The incorporation of trivalent metal cations into the LDHs structure is considered crucial for enhancing the visible light absorption, tuning the photocatalytic properties, and electronic structure of LDHs (Cr^{3+}, Fe^{3+}). Doping may substantially improve light absorption while simultaneously creating charge defects beneficial for photoinduced charge transport efficiencies.[47]

The various metal dopants alter the electronic structure of ZnAl-LDH by establishing impurity energy levels that reduce the band gap and improve absorption of visible light. The electronic

Table 2 Comparative analysis of the various modification strategies with respect to the advantages and disadvantages

Modification strategies of ZnAl-LDH	Advantages	Disadvantages
Doping	• Extends light absorption to visible wavelengths, boosting efficiency	• Greater level of dopants can reduce photocatalytic efficacy forming recombination sites
	• Promotes the separation of charge carriers to inhibit recombination	• High dopant concentrations cause agglomeration, hence minimizing surface area and active sites
	• Alters band structures to get ideal redox potentials	
Intercalation	• Intercalated molecules or anions can serve as charge-transfer bridges or mediators of electrons	• Some intercalated species can scatter light that hinders effective light penetration into LDH
	• Expose more active sites expanding interlayer space of LDH	• Certain intercalated anions or molecules can trap the charges reducing photoactivity
Calcination	• MMOs have improved electrical conductivity and higher charge separation efficiency	• Overheating can completely collapse the LDH structure
	• Robust metal–metal interaction of MMOs show higher activity	• MMOs may experience undesired phase changes at high calcination temperatures
	• Produces large-surface-area with porous structures that provide more active sites	
Heterostructure	• Can promote chemical and thermal stability and decrease photo corrosion	• Inappropriate band alignment can produce charge trapping sites encouraging electron–hole recombination
		• Heterostructure production frequently entails length, multi-step method
	• Allows band alignment which maximizes charge flow within components for desired redox reactions	• Different materials may separate or agglomerate during synthesis, resulting in uneven active sites

density of states is altered by interactions between the d or f orbitals of dopant and the O 2p or Zn 3d orbitals of ZnAl-LDH, which result in modifications to the CB and VB locations. The dopants can induce O_Vs and surface defects which create localized electronic states that improve charge mobility and surface reactivity. Dopant ions frequently serve as electron or hole traps, which lowers recombination rates and facilitates the effective separation of photogenerated charge carriers. In general, doping in ZnAl-LDH promotes charge transport, adjusts the band structure, and increases photocatalytic efficiency. Noble or transition metals like (*e.g.*, Ru, Pt, Ni, Co, Mo, Cu) can function as co-catalysts or electron carriers are more efficient for HER. These dopants with multiple oxidation states, lowers the CB edge or create donor levels to speed up electron transport for H_2 evolution. For superior pollutant degradation, the dopants like (Bi, Mn, Fe, and Cu), induce O_Vs or increase oxidative capacity by raising VB position or introducing acceptor states to boost hole activity and ROS formation.[73]

For example, Mendoza *et al.* introduced different oxidation states of Mn into ZnAl-LDH to create Mn-doped ZnAl-LDH material, which exhibited excellent 4-chlorophenol photodegradation due to the presence of various oxidation states of Mn (Mn^{2+}, Mn^{3+}, Mn^{4+}), serving as photogenerated charge separators to enhance the photocatalytic degradation of 4-chlorophenol. The introduction of Mn into the octahedral sheets improves the light-harvesting capacity of ZnAl-LDH materials. The role of Mn as a charge separator is proposed, where Mn acts as an electron e^- (Mn^{3+}, Mn^{4+}) or hole h^+ (Mn^{2+}, Mn^{3+}) trapper, depending on its oxidation state. The degradation of 4-chlorophenol is accelerated in ZAMn LDH samples due to the different Mn oxidation states (Mn^{2+}, Mn^{3+}, and Mn^{4+}) that generate an accumulation of h^+, combined with the effects of $^{\bullet}OH$ radicals, which facilitates increased degradation. Characterization techniques demonstrated the presence of Mn^{2+}, Mn^{3+}, and Mn^{4+} in the LDH structure, while the O 1s signal confirmed the LDH phase reconstruction in the aqueous medium (Fig. 8a). Mn doping of ZnAl-LDH enhances both physicochemical and photocatalytic properties.[36]

It is established that metal cation doping within the lattice structure leads to the formation of O_Vs, resulting in high catalytic performance. The role of O_Vs extends beyond enhancing light responsiveness; they can also function as e^- traps to inhibit the recombination of excitons. Hence, O_V-rich photocatalysts are particularly effective in boosting photocatalytic activity. Bismuth ions have been extensively studied in recent decades as excellent activators and sensitizers. In semiconductors, attempts have been made to enhance the density of charge carriers through Bi^{3+} doping in chalcogenide, significantly reducing the material's band gap. Due to a higher ionization potential than aluminium atoms, bismuth atoms are more likely to form Bi–O bonds. Furthermore, Bi atoms have a higher radius than aluminium atoms, leading to the distortion of lattice and the formation of O_Vs. By doping ZnAl-LDH with Bi, Wang *et al.* designed Bi-doped ZnAl-LDH enriched with O_Vs through the hydrothermal method. The increased concentration of O_Vs at the material's surface *via* Bi^{3+} doping in Bi–ZnAl-LDHs enhanced natural light absorption ability and the efficiency of photogenerated electron/hole pair separation,

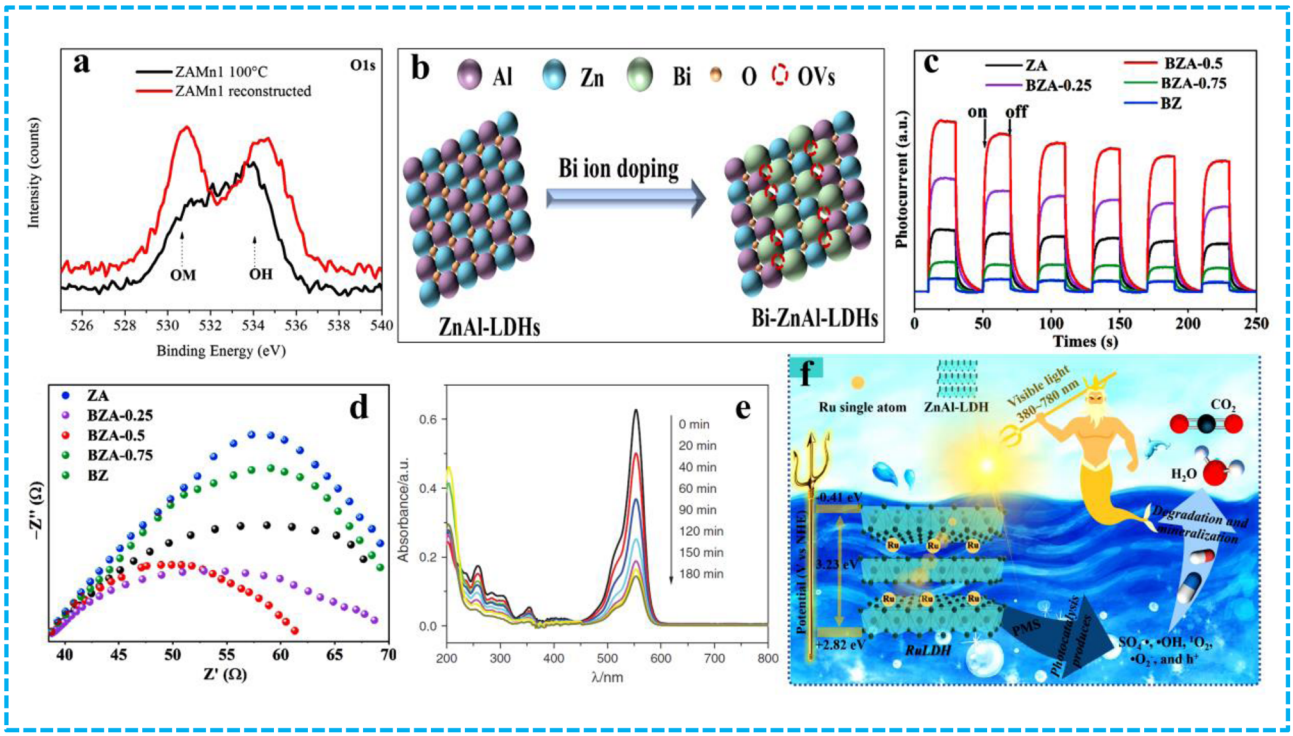

Fig. 8 (a) XPS spectra of the O 1s region of ZAMn1 dried sample, reproduced with permission from Elsevier. Copyright © 2015.[36] (b) Schematic illustration of the vacancy formation of BZA-*X*, (c) the TPC response, (d) Nyquist impedance plots of BZA-*X*, reproduced with permission from Royal Society of Chemistry. Copyright © 2024.[56] (e) UV-visible spectra of RhB solution irradiated under visible light over the sample Cu-1.0, with permission from American Scientific Publishers. Copyright © 2019.[74] (f) Mechanistic pathway in RuLDH0.2/PMS/vis system, reproduced with permission from Elsevier. Copyright © 2024.[75]

influencing the degradation rate of ciprofloxacin (CIP). The substitution of Bi in ZnAl-LDH successfully promoted the creation of abundant surface O_Vs. The O_Vs induced by Bi substitution facilitated the process of H^+ adsorption in the reaction system, further enhancing the OH formation (Fig. 8b). The primary active species, OH^- and h^+, significantly assisted in the photodegradation of CIP, with the degradation rate constant for BZA-0.5 being 1.56 and 2.63 times greater than those of ZnAl-LDH, respectively. BZA-0.5 demonstrates outstanding catalytic activity for CIP degradation across a broad pH range. The spike in the concentration of O_Vs contributed to the production of ROS, subsequently improving the material's photocatalytic activity. A potential reaction mechanism was proposed in which BZA-*X* adsorbs oxygen and H^+ to generate H_2O_2, producing $^-$OH as the active substance. EPR experiments further validated that OH^- and h^+ were the primary active substances. Ultimately, the authors explained that the unique structural features, larger specific surface area, and active multicomponent in the Bi-doped ZnAl-LDH nanocomposite substantially enhance the photocatalytic degradation of CIP, based on the separation efficiency of the photogenerated charge carriers, as corroborated by photocurrent density and electrochemical impedance spectra (EIS), as shown in Fig. 8c and d.[56] Li *et al.* adopted the coprecipitation method to incorporate Cu into ZnAl-LDH, which imparts O_V, and generates distorted CuO_6 octahedrons. These well-defined sheets contribute to the electronic excitation under visible light. The doping of Cu^{2+} into the LDH sheets expands the visible light absorption capability of ZnAl-LDH (Fig. 8e). The doped Cu^{2+} ions also act as photo-induced charge carrier separators, efficiently separating the excited electron–hole pairs. This results in outstanding photodegradation of RhB and stability that fits the first-order kinetics model.[74]

Similarly, Zheng *et al.*, combined the optimized amount of ruthenium (Ru) doped into ZnAl-LDH, which caused enhanced photocatalytic activities. The generation of O_Vs was one among the characteristics that decreased charge recombination and improved adsorption. It is known that the copious 4f electrons of lanthanides integrated as dopants that can segregate photogenerated charges by distorting the LDH lattice and serve as potent adsorption sites for reactants. The optimized catalyst, noted as RuLDH0.2, displayed outstanding catalytic efficiency during the PMS activation for the tetracycline degradation, achieving 100% degradation within 35 min, accompanied by a 45% mineralization of TC within 45 min. The RuLDH catalyst owns copious catalytic reaction sites and displays visible light trapping ability, promoting its utilisation in TC photodegradation. RuLDH0.2 nanoarrays with single-atom synergy were the main photoreactive elements in photoactivated peroxymonosulfate (PMS). The RuLDH0.2 structures' well-matched single atoms contributed to a favourable balance between light-capturing capacity and high redox potential, enabling an array

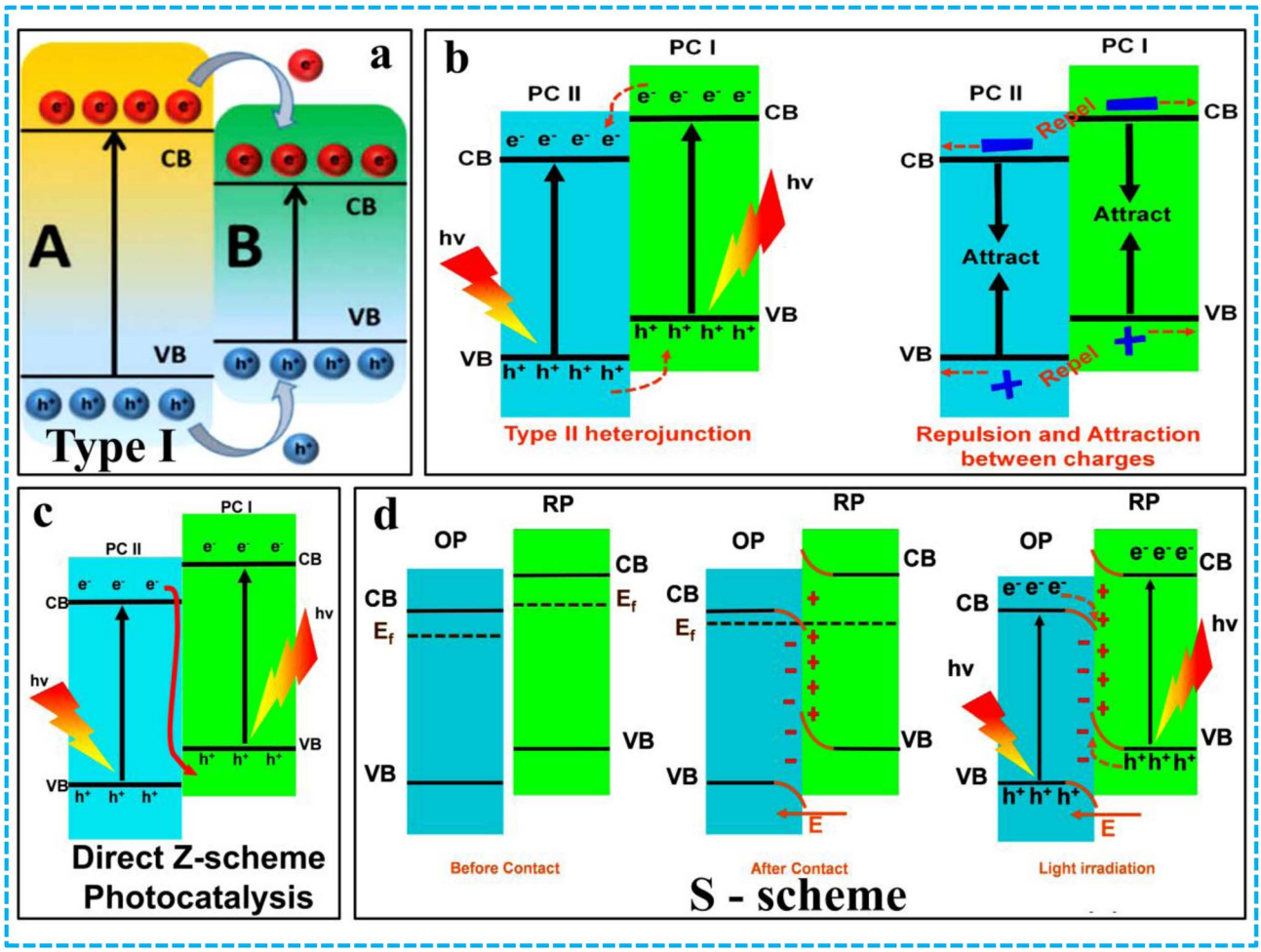

Fig. 9 Schematic representation of (a) type I, reproduced with permission from Taylor & Francis. Copyright © 2020.[78] (b) Type II, (c) direct Z-scheme, and (d) S-scheme heterostructures in photocatalysis, reproduced with permission from Elsevier. Copyright © 2024.[8]

of applications in TC removal and monitoring as depicted in the mechanism present in Fig. 8f.[75]

5.2. ZnAl-LDH-based heterostructures for photocatalysis

Photocatalytic heterostructures have emerged as one of the most effective strategies to overcome the intrinsic limitations of single-component semiconductors, such as rapid e^-/h^+ recombination and limited light absorption. By coupling two or more semiconductors with different band structures, it is possible to create built-in electric fields at the interface, which facilitate efficient charge separation and transfer. This interfacial engineering significantly enhances photocatalytic activity, making several heterojunctions a central design principle in advanced photocatalyst development, each with distinct charge transfer mechanisms and performance characteristics. For example, in type-I heterojunctions, both photogenerated electrons and holes migrate into one semiconductor with a narrower band gap. While this structure favours strong light absorption, it often suffers from poor redox efficiency due to high charge carrier recombination. Type-II heterojunctions enable spatial separation of charge carriers—electrons move to the conduction band of one component while holes remain in the valence band of the other—thereby extending carrier lifetime. However, this configuration usually results in a loss of redox potential, which can limit reaction kinetics. Z-scheme heterojunctions, inspired by natural photosynthesis, combine strong redox ability with efficient charge separation by allowing high-energy electrons and holes to remain in their respective bands while recombining low-energy carriers at the interface. Their main drawback lies in structural complexity and the requirement for precise band alignment to maintain directional charge flow. More recently, S-scheme heterojunctions have gained attention for integrating the advantages of type-II and Z-scheme systems. They rely on an internal electric field and band bending to drive selective charge transfer, maintaining both high redox power and effective charge separation. Despite their promise, their practical application is often challenged by the difficulty in achieving stable and well-defined interfaces. While each heterojunction type brings unique strengths, they also present specific trade-offs related to charge recombination, redox potential, and fabrication complexity. Hence, a clear understanding of these mechanisms is essential for rational design, enabling the development of next-generation photocatalysts with superior activity and stability (Fig. 9).[76,77]

ZnAl-LDH has garnered a lot of research attention in the photocatalysis arena, primarily because of its superior physicochemical characteristics, including strong response to visible and ultraviolet light, wide specific surface area, high capacity for adsorption, and tunable band gap. However, the quick recombination of photogenerated charge carriers of ZnAl-LDH decreases its photocatalytic activity, which confines its use as a standalone photocatalyst. Integrating ZnAl-LDH with other semiconductor materials with matching energy levels enables the charge transfer process mediated by either type-I, type-II, Z-scheme, or S-scheme mechanism. The ZnAl-LDH-based heterostructures enhanced performance by enabling efficient charge separation through heterojunctions, reducing electron–hole recombination, and broadening light absorption across the UV-visible spectrum. The integration of materials improves charge mobility, increases surface area and active sites, and provides synergistic effects that augment catalytic activity. Additionally, composite structures offer greater stability against photo corrosion and allow tunable physicochemical properties, making them highly effective for various photocatalytic applications such as pollutant degradation and hydrogen generation, *etc.*

For instance, Wang *et al.*, reported MoO_3/ZnAl-LDH heterostructure for the degradation of tetracycline (TC) *via* photocatalysis. The coupling of MoO_3 (10 wt%) and ZnAl-LDH using solvent evaporation method causes effective partition of photogenerated carrier charge pairs, and the resultant high-performance MoO_3 (10 wt%)/ZnAl-LDH heterostructure revealed an efficiency in TC removal of 90.5% in 60 min over MoO_3, and maintained outstanding recycling capacity and stability after five repeated cycles. The author also anticipated a possible type-II mechanism (Fig. 10a) for promoting charge separation among MoO_3 and ZnAl-LDH, for the enhanced photocatalytic property of the composites (Wang *et al.*, 2021), as witnessed from the transient photocurrent and EIS spectra (Fig. 10b and c).[45]

As heterostructure formation is an efficient method for increasing the photocatalytic activity of composite by accelerating photogenerated charge migration. In this framework, Sun *et al.* successfully synthesized flower-like spherical ZnCdS/Bi_2WO_6/ZnAl-LDH dual type-II heterostructure using a two-step hydrothermal process for crystalline violet (CV) degradation and photocatalytic hydrogen production. The intimate connection of the three components ZnCdS, Bi_2WO_6, and ZnAl-LDH leads to the creation of the dual type-II heterostructure that facilitates photo-induced carrier separation and transfer between the three components, reducing the recombination rate for effective photocatalytic activity of ZnCdS/Bi_2WO_6/ZnAl-

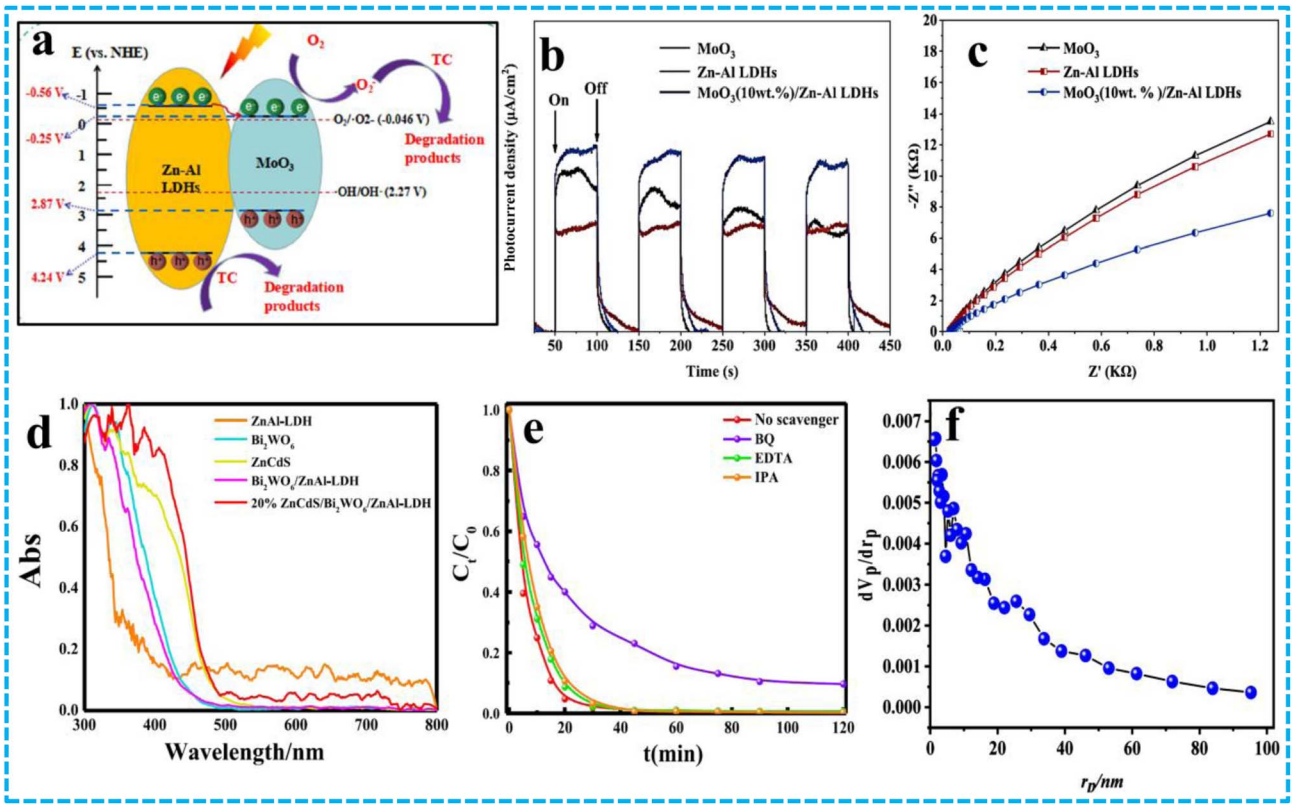

Fig. 10 (a) Visible light irradiated photocatalytic degradation mechanism for TC over MoO_3/Zn–Al LDHs composites, (b) transient photocurrent responses, and (c) electrochemical impedance spectroscopy (EIS) chart of MoO_3, Zn–Al LDHs, and MoO_3 (10 wt%)/Zn–Al LDHs composite, reproduced with permission from Elsevier. Copyright © 2021.[45] (d) UV-vis/DRS absorption spectra of ZnCdS, Bi_2WO_6, ZnAl-LDH, Bi_2WO_6/ZnAl-LDH composites, and ZnCdS/Bi_2WO_6/ZnAl-LDH composites, (e) simulated sunlight irradiated experimental results of 20% ZnCdS/Bi_2WO_6/ZnAl-LDH through radical trapping test, reproduced with permission from Elsevier. Copyright © 2023.[79] (f) Pore size distribution plot of Fe_3O_4–SiO_2-EN@Zn–Al-LDH, reproduced with permission from Elsevier. Copyright © 2024.[80]

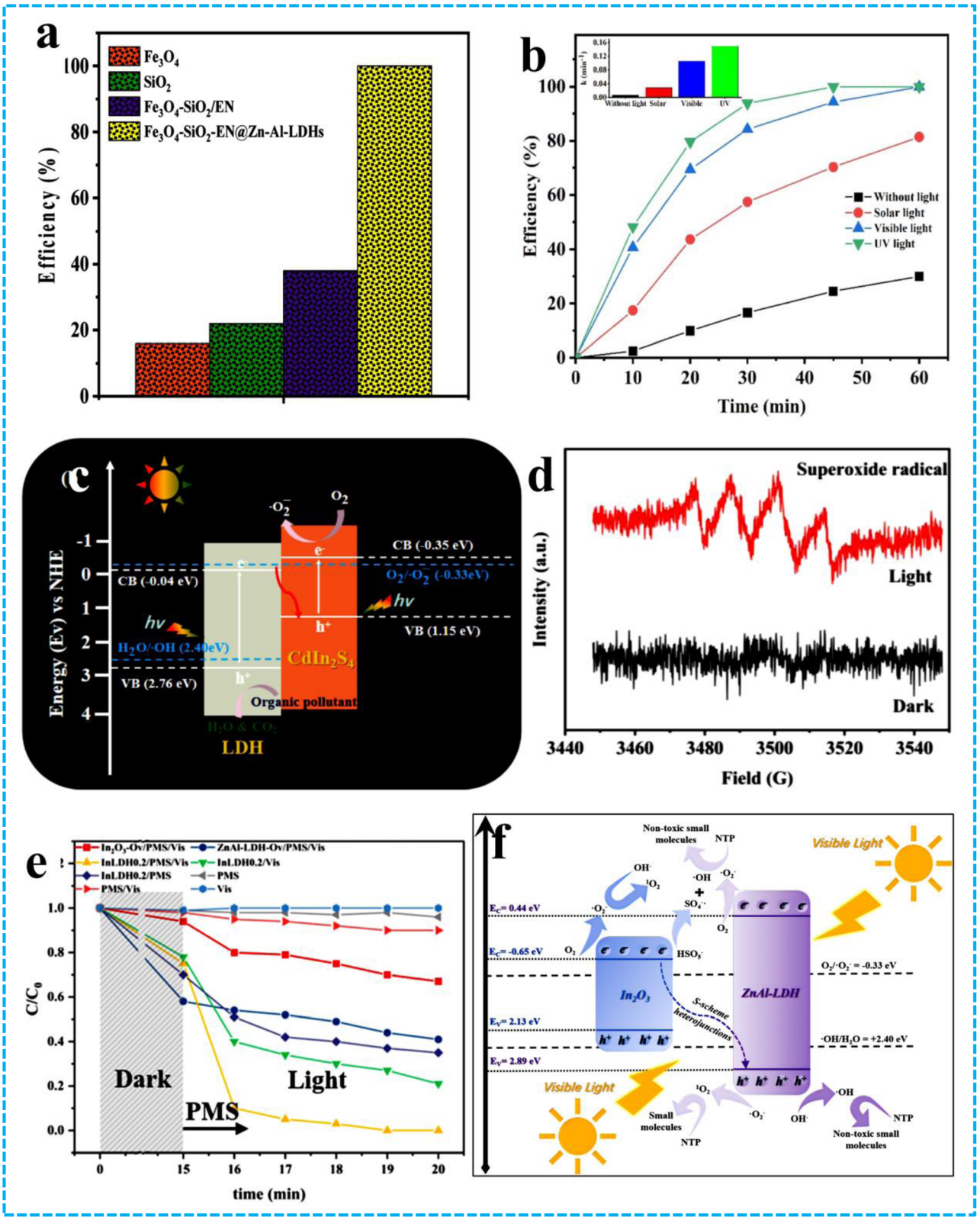

Fig. 11 (a) CIP removal rate in Fe_3O_4–SiO_2-EN@Zn–Al-LDH, (b) under different light sources, reproduced with permission from Elsevier. Copyright © 2024.[80] (c) Photogenerated Z-scheme carrier transfer path diagram of $CdIn_2S_4$/LDH heterojunction, (d) DMPO spin-trapping ESR spectra for 15 wt% $CdIn_2S_4$/LDH in aqueous dispersion for DMPO-$^{\bullet}O_2^-$, reproduced with permission from Elsevier. Copyright © 2025.[81] (e) Efficiency of NTP removal, and (f) NTP degradation mechanism in In_2O_3-O_V/ZnAl-LDH-O_V/PMS/vis system, reproduced with permission from Elsevier. Copyright © 2025.[82]

LDH heterostructure. The UV-DRS analysis (Fig. 10d) of 20% $ZnCdS/Bi_2WO_6$/ZnAl-LDH manifests the highest redshift in visible light and a smaller band gap, which is due to the strong light absorption of ZnCdS and Bi_2WO_6, anticipated to have the best photocatalytic activity. The $ZnCdS/Bi_2WO_6$/ZnAl-LDH heterostructure showed a superior photocatalytic CV degradation within 40 min, and H_2 evolution rate of 633.58 μmol g^{-1}, which is 8-fold times higher than pure ZnAl-LDH. The high activity of 20% $ZnCdS/Bi_2WO_6$/ZnAl-LDH was attributed to the synergistic effects of heterointerfaces. Further radical trapping tests involving BQ (benzoquinone), EDTA (ethylene diamine tetra acetic acid), and IPA (isopropyl alcohol), as illustrated in Fig. 10e indicated superoxide ($O_2^{\bullet -}$) as the primary active species in the photocatalytic degradation of CV based on the superoxide radical trapping with the help of BQ.[79]

Following the concept of nanostructure design, T. J. Al-Musawi *et al.* designed the Fe_3O_4–SiO_2-EN@Zn–Al-LDH nanostructure, which functions as a novel photocatalyst for the degradation of CIP. The advantageous electrical interaction among the positive charges of LDH and the negative charges of Fe_3O_4–SiO_2 and the high conductivity of Fe_3O_4 nanoparticles allows them to function as an electron acceptor generated from the LDH surface for separating e^-/h^+ pairs and prolonging the lifespan of these species for photocatalytic activity. The composite material possesses notable BET surface area (28.67 m^2 g^{-1}), large pore volume (6.58 cm^3 g^{-1}), and small average pore size (1.64 nm) as evident in Fig. 10f. The core–shell LDH composite demonstrated the ease of activation in various light sources, and it can eliminate CIP by 81.4% in visible light, 99.9% in UV light, and 99.9% in solar light (Fig. 11a and b). These superior outcomes are due to the effect of the composite's large surface area and unique chemical properties.[80] M. Sun *et al.* designed a novel Z-scheme-based heterostructure, such as $CdIn_2S_4$/ZnAl-LDH composites, *via* the mechanochemical process for the photodegradation of sodium isopropyl xanthate (SIPX). The high CB potential of $CdIn_2S_4$ and the lower band positions of ZnAl-LDH enable the construction of Z-type heterojunctions, achieving full carrier transfer and separation. The $CdIn_2S_4$/LDH composite has an absorption edge between 780 and 830 nm, indicating improved light absorption for photocatalytic degradation of SIPX as compared to pure ZnAl-LDH and $CdIn_2S_4$. The optimized 15 wt% $CdIn_2S_4$/LDH composite achieved over 90% degradation in 180 minutes. The enhanced activity is due to a stable Z-scheme heterojunction structure depicted in Fig. 11c, which boosts light absorption and stimulates charge separation, facilitating photocatalytic stability and efficiency. DMPO spin trapping analysis revealed strong signals corresponding to the $^{\bullet}O_2^-$ (Fig. 11d) upon exposure to light, playing an inevitable role in the reaction.[81] For the design of high-performance catalysts, Z. Zeng *et al.* developed an ultrathin 2D/2D heterostructure of In_2O_3-O_V/ZnAl-LDH-O_V (InLDH0.2) by electrostatic self-assembly of In_2O_3 with O_Vs (In_2O_3-O_V) and oxygen-deficient ZnAl-LDH nanosheets (ZnAl-LDH-O_V) for superior nitenpyram (NTP) degradation. The In_2O_3-

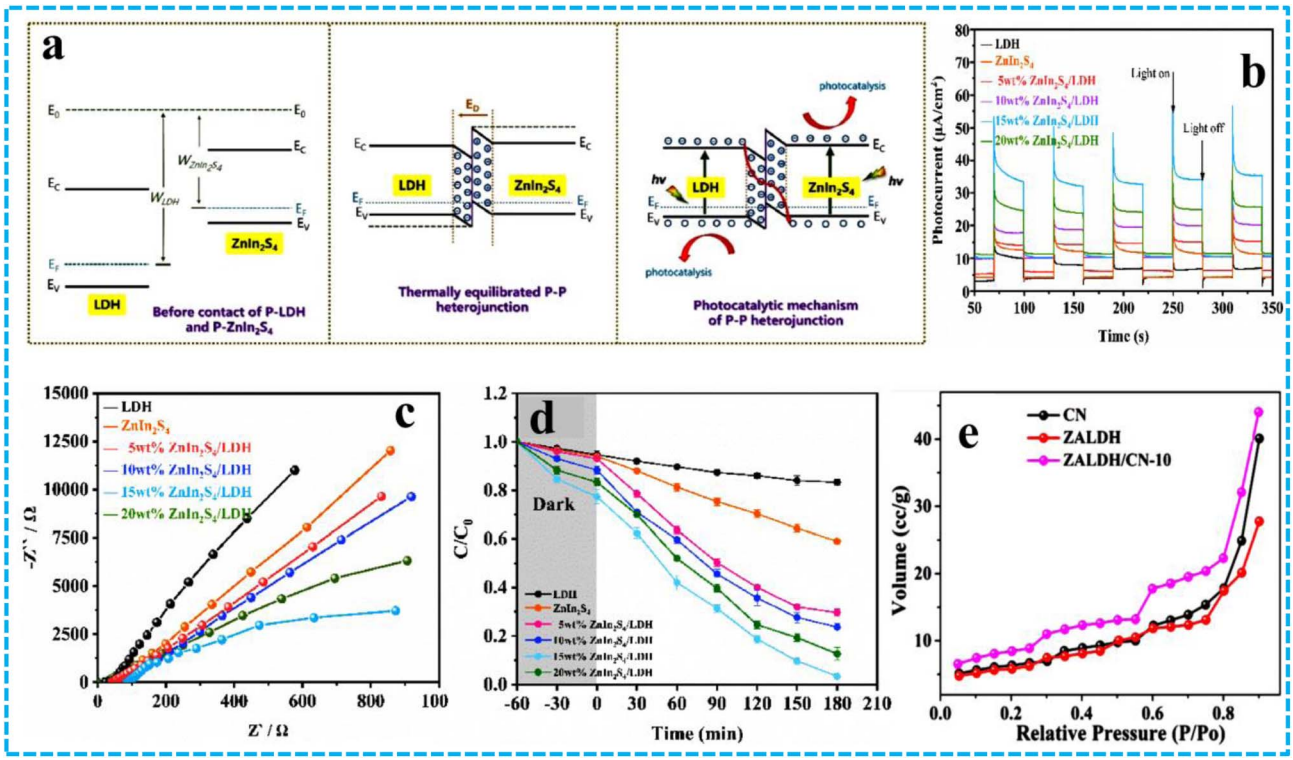

Fig. 12 (a) Energy-band sketch of the heterojunctions combined by Zn–Al LDH, and $ZnIn_2S_4$ and (b) transient photocurrent response, and (c) EIS spectra of Zn–Al LDH, $ZnIn_2S_4$, and *n* wt% $ZnIn_2S_4$/LDH samples, (d) degradation of SIPX with time using *n* wt% $ZnIn_2S_4$/LDH samples, reproduced with permission from Elsevier. Copyright © 2024.[83] (e) N_2 adsorption isotherm of pure CN, pure ZALDH, and composite of ZALDH/CN-10, reproduced with permission from Elsevier. Copyright © 2024.[84]

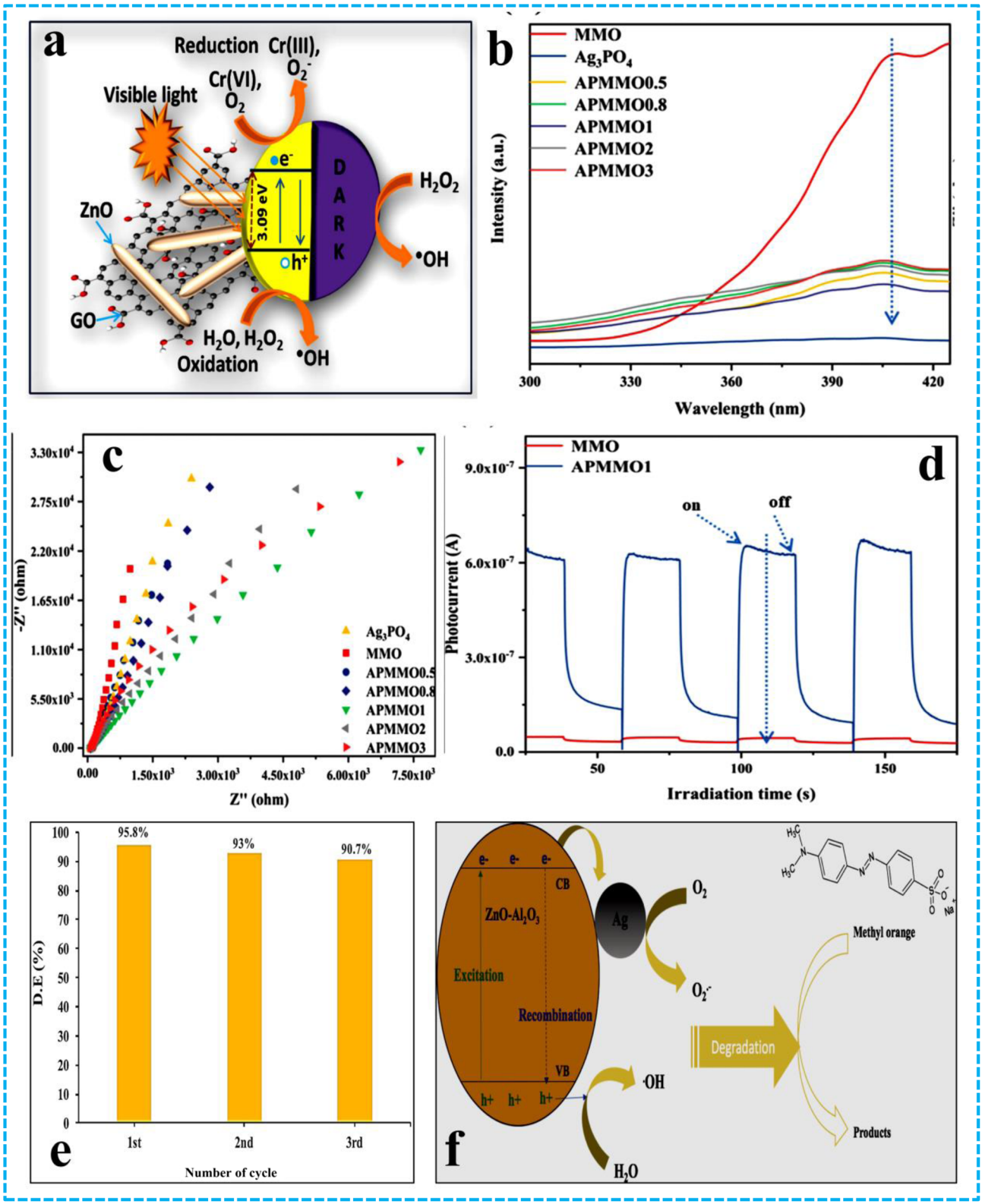

Fig. 13 (a) Proposed degradation mechanism for MB and Cr(VI) reduction over ZnO/GO, reproduced with permission from Elsevier. Copyright © 2024.[61] (b) PL spectra of Ag_3PO_4, MMO, APMMO0.5, APMMO0.8, APMMO1, APMMO2, and APMMO3, (c) EIS and (d) photocurrent response spectra of MMO and APMMO1, reproduced with permission from Elsevier. Copyright © 2022.[63] (e) Reusability test, and (f) degradation pathway over the surface of the Ag–ZnO–Al_2O_3 photocatalyst, reproduced with permission from Elsevier. Copyright © 2023.[85]

O_V/ZnAl-LDH-O_V with rich O_V, enhanced light absorption (450–550 nm) facilitates effective transfer of photoinduced electrons to oxygen molecules to create highly reactive singlet oxygen ($^1O_2$) for enhancing the electronic conductivity. The creation of heterointerface chemical bonds (Al–O–In) is greatly aided by O_Vs, which lead to the delocalization of electrons surrounding the indium sites. In contrast, the InLDH0.2 sample exhibited markedly superior performance in the PMS/vis system, as evident in Fig. 11e, achieving complete (100%) NTP degradation, compared with 76.9% for ZnAl-LDH-O_V and only 33% for In_2O_3-O_V, while also attaining a mineralization efficiency of 47%. Furthermore, the ultrathin S-scheme heterojunction (Fig. 11f) facilitates the efficient formation of $^{\bullet}OH$, $SO_4^{\bullet-}$, and $^1O_2$ radicals and promotes the activation of PMS by encouraging the flow of photogenerated electrons from In_2O_3-O_V to the Al sites of ZnAl-LDH-O_V for enhanced photocatalytic degradation.[82]

In another attempt, M. Sun *et al.* created an innovative binary Z-scheme $ZnIn_2S_4$/ZnAl-LDH composite using a ball-milling process and a two-step mechanochemical approach.[83] This $ZnIn_2S_4$/ZnAl-LDH composite showed exceptional efficiency in the photodegradation of the organic flotation reagent sodium isopropyl xanthate (SIPX) under sunlight, establishing the Z-scheme heterojunction. The optimal 15 wt% $ZnIn_2S_4$/LDH composite discloses 95% xanthate (SIPX) degradation within 180 min under visible light, which was approximately 18.2 and 5.0 times that of LDH and $ZnIn_2S_4$. The superior photocatalytic activity of $ZnIn_2S_4$/LDH hybrid is initiated from the P–P, Z-scheme heterojunction as verified from the energy band sketch diagram, photocurrent, EIS, and results (Fig. 12a–c). Besides, the quantitative photocatalytic results reveal a pronounced enhancement in the $ZnIn_2S_4$/LDH heterojunction system, with the optimized 15 wt% $ZnIn_2S_4$/LDH sample achieving 95% SIPX degradation, a 5-fold increase compared to the LDH and 2.5-fold increase compared to $ZnIn_2S_4$, clearly demonstrating the superior synergistic interaction (Fig. 12d).

As is well known, the LDHs have been incorporated onto various substrates such as metal oxide, g-C_3N_4, metal sulphide (ZnS), and MOF materials for heterostructure formation towards photocatalytic applications. A. Gandamalla *et al.* reported the coupling of extremely effective ZnAl-LDH with g-C_3N_4 (ZALDH/CN) heterostructure for ciprofloxacin (CIP) photodegradation using a microwave irradiation approach. Compared to neat CN and ZALDH photocatalysts, the optimum ZALDH/CN-10 composite demonstrated a higher degradation of 84.10% with rate constant of 1.22×10^{-2} min^{-1}. The ZALDH/

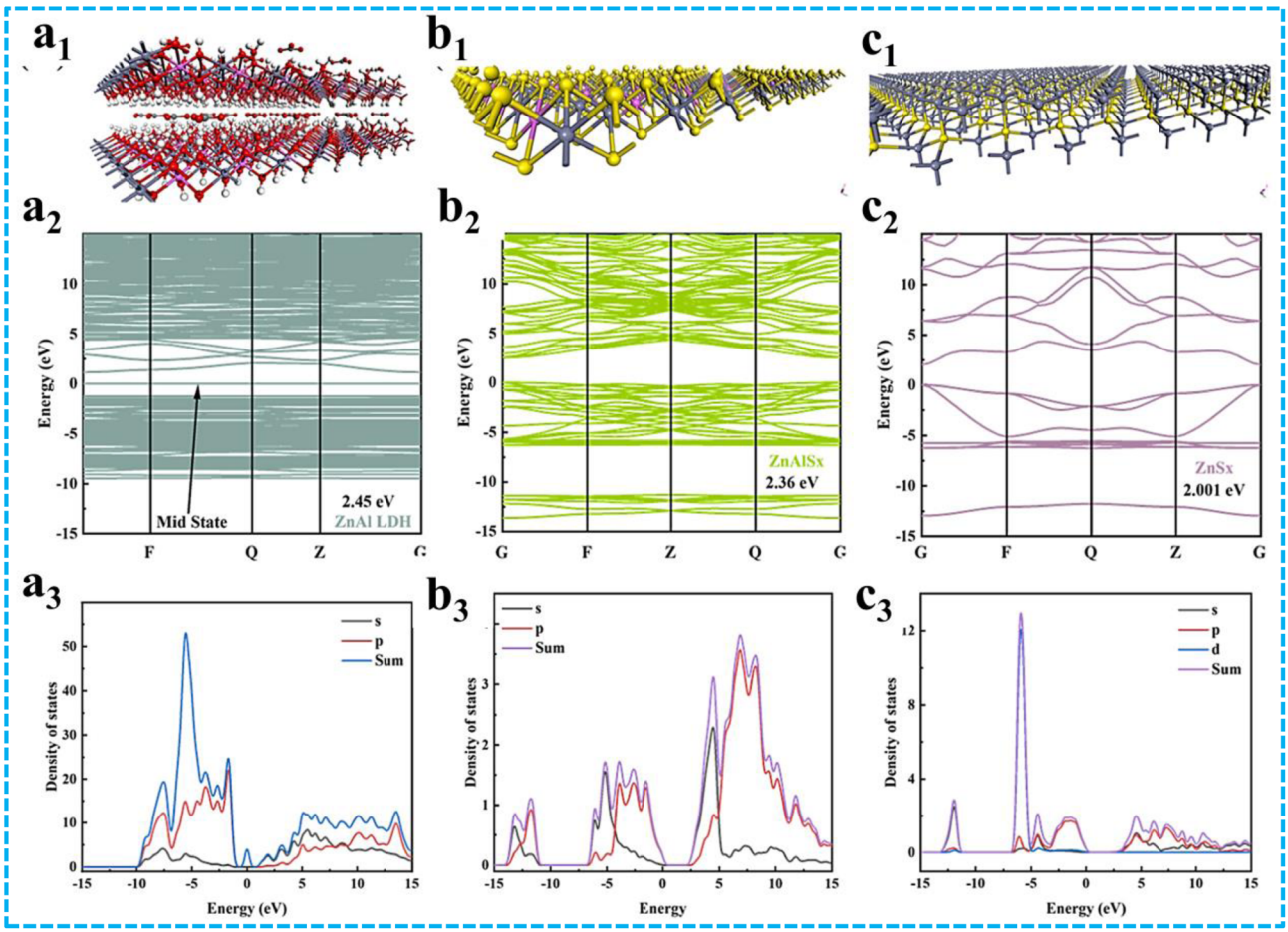

Fig. 14 (a1–c1) Structural models, (a2–c2) band structures, and (a3–c3) total PDOS of ZnAl LDH, $ZnAlS_x$, and ZnS_x, reproduced with permission from American Chemical Society. Copyright © 2024.[86]

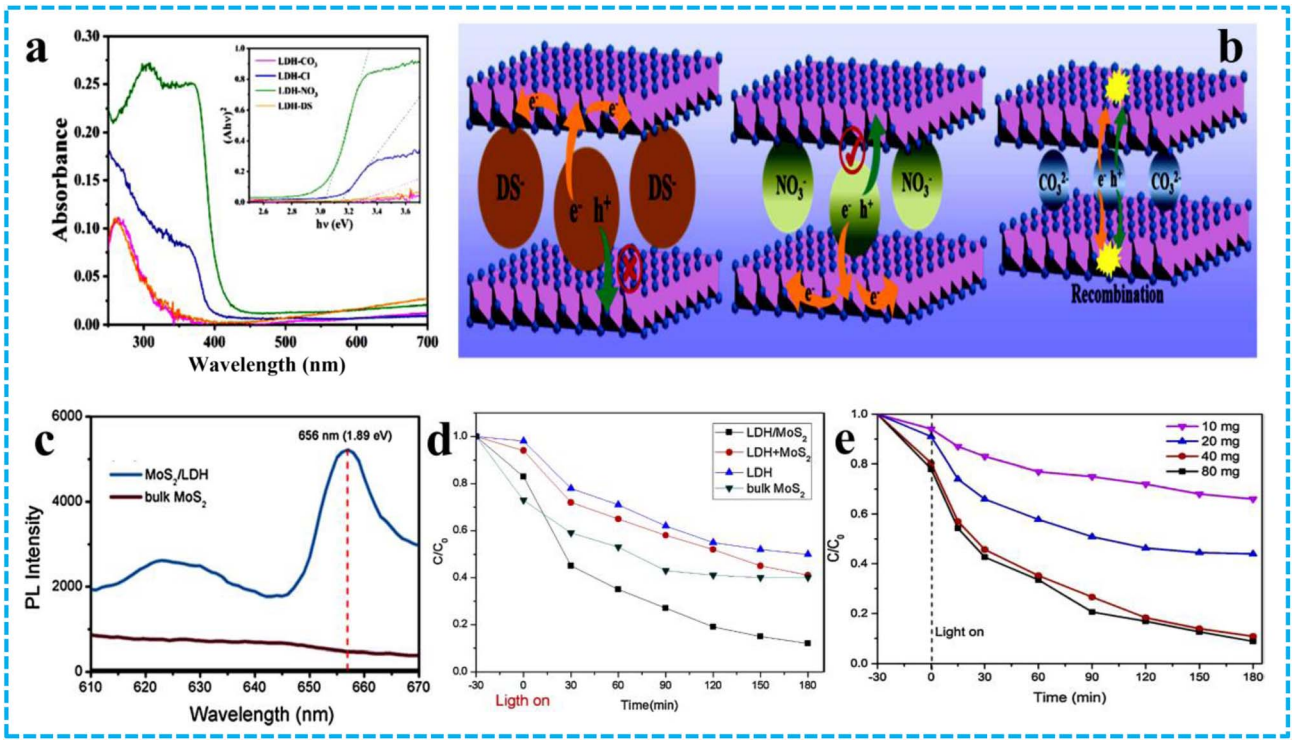

Fig. 15 (a) UV-vis DRS spectra of LDH-CO_3, LDH-Cl, LDH-NO_3, and LDH-DS, respectively, (b) schematic illustration of LDH-DS, LDH-NO_3, and LDH-CO_3, respectively, reproduced with permission from Elsevier. Copyright © 2024.[89] (c) PL spectroscopy for pristine MoS_2 and MoS_2/LDH nanocomposite, (d) photocatalytic efficiency of various synthesised catalyst, followed by (e) effect of composite dosage on the photocatalytic efficiencies, reproduced with permission from Royal Society of Chemistry. Copyright © 2020.[56]

CN-10 composite material illustrated a strong synergistic impact with a higher specific surface area of 23.60 $m^2\ g^{-1}$ (Fig. 12e) than pure CN (17.60 $m^2\ g^{-1}$), ZALDH (16.17 $m^2\ g^{-1}$). Radical experiments specified $^{\bullet}OH$ as the dominant reactive species. The heterojunction formed between LDH and CN, interacted by surface hydroxyl groups and π-electron cloud interactions, promoted efficient charge separation.[84] Alternatively, the semiconducting properties of MOFs with high porosity are used to serve as effective photocatalysts for various applications. In this context, A. Chakraborty *et al.* designed ZnAl-LDH/MOF-5 nanocomposite which assisted the growth of MOF-5 crystals on ZnAl-LDH layers, along with *in situ* nucleation and depicted a superior anionic dye removal methyl orange (MO) rate of 99.98% after 40 min. The MOF particles can be enabled to grow epitaxially on the surface of LDH with the assistance of its surface unsaturated coordination sites enhancing surface defects, red-shifted light absorption, and improving ROS production ($^{\bullet}OH$, $O_2^{\bullet-}$) generation under sunlight. The ZnAl-LDH/MOF-5 hybrid enhances the production of OH radicals, allowing dye molecules to break down into CO_2, H_2O, and additional products due to LCCT (linker-to-cluster charge transfer) processes.[39]

Alternatively, the derived ZnAl-LDH-based heterostructure has a substantial effect on photocatalytic activity as photocatalytic systems due to significant physicochemical properties. For this, D. A. Islam *et al.* proposed a promising alternative utilizing ZnAl-LDH precursors and used an innovative *in situ* chemical decomposition (low-temperature pyrolysis) to create ZnO nanorods on graphene oxide (GO) nanosheets, which can form high-performance ZnO/GO composites.[61] At first, ZnAl-LDH/GO composite was synthesized through the LDH's *in situ* growth on the GO nanosheets. Secondly, thermal decomposition of ZnAl-LDH/GO nanocomposite at 80 °C formed homogeneously dispersed size-controlled ZnO nanorods on GO nanosheets. The narrow band gap energy in ZnO/GO nanocomposites showed outstanding photocatalytic activity for Cr(VI) reduction and methylene blue degradation under visible light exposure. The improved photocatalytic performance of ZnO/GO composites was owing to the crucial role of GO in controlling the directional growth of ZnO nanorods through the collective electron–hole transfer effect for the potential wastewater remediation (Fig. 13a). Similarly, J. Zheng *et al.* prepared Ag/Ag_3PO_4/calcined ZnAl-LDH (MMO) (APMMO/PDS/vis) system and evaluated the nitenpyram (NTP) degradation. The heterojunction formation between ZnAl-LDH (MMO) and Ag_3PO_4 may intensify the photogenerated e^-/h^+ separation process and inhibit the recombination efficiency, thereby increasing the NTP photodegradation efficiency *via* peroxydisulfate (PDS)-based photocatalytic activation methods. Under optimal conditions, the APMMO1/PDS/vis system attains complete NTP removal within 30 minutes. PDS produces $SO_4^{\bullet-}$ and hydroxyl radicals, with a higher oxidation potential that enhances catalytic activity. The integration of MMO increases surface area for active site exposure, thereby refining the photocatalytic performance. Further PL, EIS, and photocurrent study (Fig. 13b–d) also validate that Ag_3PO_4 MMO, and APMMO1 can activate PDS

for the photocatalytic degradation of NTP under visible light.[63] Recently, F. Z. Janani *et al.*, assessed the photocatalytic performance of methyl orange (MO) degradation under UV irradiation using Ag–ZnO–Al_2O_3 heterostructure derived from the calcination of Ag-doped ZnAl-LDH *via* a solid-state process. The Ag–ZnO–Al_2O_3 photocatalyst maintained good recycling stability as depicted in Fig. 13e with high MO photodegradation performance of 90.7% which is due to the doping effect of Ag metal. The presence of Ag metal functions as a photogenerated electrons acceptor agent on the catalyst surface, and contributes to the excellent photodegradation performance (Fig. 13f). These showed that the addition of the Ag metal to the LDH matrix increases the charge movement and prevents the recombination of photogenerated exciton pairs, resulting in a markedly amended photocatalytic activity.[85]

Furthermore, Hu *et al.* suggest a distinctive *in situ* topological vulcanization technique for maximizing the ZnAl-LDH-derived sulfides ($ZnAlS_x$) for photocatalytic hydrogen production. The as-synthesized ZnS_x with abundant active sites exhibits superior photocatalytic activity for hydrogen production (11.89 mmol g^{-1} h^{-1}) and tetracycline degradation (91.94%) under light illumination. The DFT analysis as illustrated in Fig. 14, established that the optimized surface electronic properties and energy band structure of derived ZnAl-LDH, improving carrier separation, which in turn increases photooxidative and reductive capability. Further the higher crystallinity and larger specific surface area of ZnS_x with copious active sites supports the superior photocatalytic activity over hydrogen production and degradation activity compared to the pristine ZnAl-LDH and $ZnAlS_x$.[86]

5.3. Intercalated ZnAl-LDH structures for photocatalytic performances

Generally, layered intercalation materials (LIMs) are formed by weakly bonded layers of 2D layered materials separated by van der Waals (VDW) gaps. These gaps permit the chemical intercalation of foreign atoms, ions, or molecules without rupturing the strong in-plane covalent bonds, resulting in unique chemical and physical characteristics.[87] The physico-chemical properties of LDHs can be significantly altered by intercalation, especially when used as photocatalysts. This process can modify their band gap, increase porosity and surface area, and improve structural and chemical stability, leading to better charge separation and migration, which alters the photocatalytic reaction pathway. Replacing anions in the interlayer adjusts the crystal structure of LDHs, enhancing catalytic performance.[88] During redox processes, intercalated species can improve selectivity, increase adsorption of target molecules, and introduce redox-active groups, boosting durability and recyclability of the photocatalyst. In 2024, Z. Hao and colleagues designed ZnAl-LDH intercalated with various anions, including CO_3^{2-}, Cl^-, NO_3^-, and DS^-, prepared *via* nucleation and recrystallization, to investigate their photocatalytic CO_2 reduction. Differences in interlayer spacing caused by different intercalated ions influenced their photocatalytic activity, despite similar crystallinity and shape. Among these, LDH-NO_3^- with an interlayer spacing of 0.88 nm showed the highest photocatalytic CO_2 reduction ability, with a CO generation rate of 3.80 μmol g^{-1} h^{-1} and outstanding selectivity (78.4–94.2%). LDH-NO_3^- demonstrated the highest rate of CO production, significantly surpassing the others. Physicochemical analyses revealed that ZnAl-LDH samples have moderate UV absorbance (240–330 nm) and band gaps from 3.01 to 3.18 eV, likely due to interlayer anions acting as chromophores, influencing photocatalytic activity (Fig. 15a). These findings highlight the significance of choosing appropriate interlayer anions for designing effective LDH-based photocatalysts, as shown in Fig. 15b. The elemental states in ZnAl-LDH samples result in better photocatalytic CO_2 reduction, with LDH-NO_3^- exhibiting higher performance. A smooth electron transfer within the [MO_6] units of the brucite-like layers of ZnAl-LDH is suggested by the higher surface oxygen vacancy percentage and the lower binding energy of Zn^{2+} in ZnAl-LDH-(NO_3^-), facilitating charge transfer and stability. XRD analysis confirmed LDH-NO_3^- as the most effective and durable catalyst, demonstrating its structural stability.[89] To augment visible light absorption by adjusting the band gap and leveraging the synergistic properties of related materials, S. Chen *et al.* developed MoS_2-intercalated ZnAl-LDH hydrotalcite through coprecipitation and hydrothermal methods. LDH restricts MoS_2 growth and favours the formation of the highly conductive and active 1T phase of MoS_2, which contains about 68.3% of the material due to confinement within the LDH layers. Excess electron doping from intercalated 1T-MoS_2 can induce structural phase transitions in the LDH host, fundamentally altering its properties. The MoS_2/LDH composite shows significant promise for photocatalytic decomposition of methylene blue, primarily due to heterostructure construction between MoS_2 and ZnAl-LDH. This composite exhibit increased visible light absorption caused by MoS_2 exfoliation and band structure modifications. PL analysis in Fig. 15c indicates a stronger emission peak (~656 nm), reflecting more defect sites than bulk MoS_2, which enhances photocatalytic activity. The methylene blue degradation rate was markedly improved in the presence of MoS_2/LDH composites, indicating that the material is not a simple physical mixture, but involved chemical interactions between MoS_2 and LDH, and their integration results in a synergistic enhancement of photocatalytic activity (Fig. 15d). Also, the degradation efficiencies underwent an upward increase with the increasing dosage of catalyst up to 40 mg (Fig. 15e) beyond which increasing the dosage increases the light scattering which drastically affects the photocatalytic efficiency.[56]

5.4. Interpretation of piezo potential mediated photocatalytic pollutant degradation

Piezo catalytic materials, such as 1D (ZnO nanorods, $BaTiO_3$ nanofibers), and 2D nanostructures (MoS_2 layers, BiOCl nanosheets, and $Bi_4Ti_3O_{12}$ nanosheets), can deform under mechanical force, generating piezo-polarized fields leading to increased catalytic activity. Likewise, ZnAl-LDH also possess the unique advantage of a tailored band structure *via* metal cation doping for enhanced visible light absorption capability, adaptable

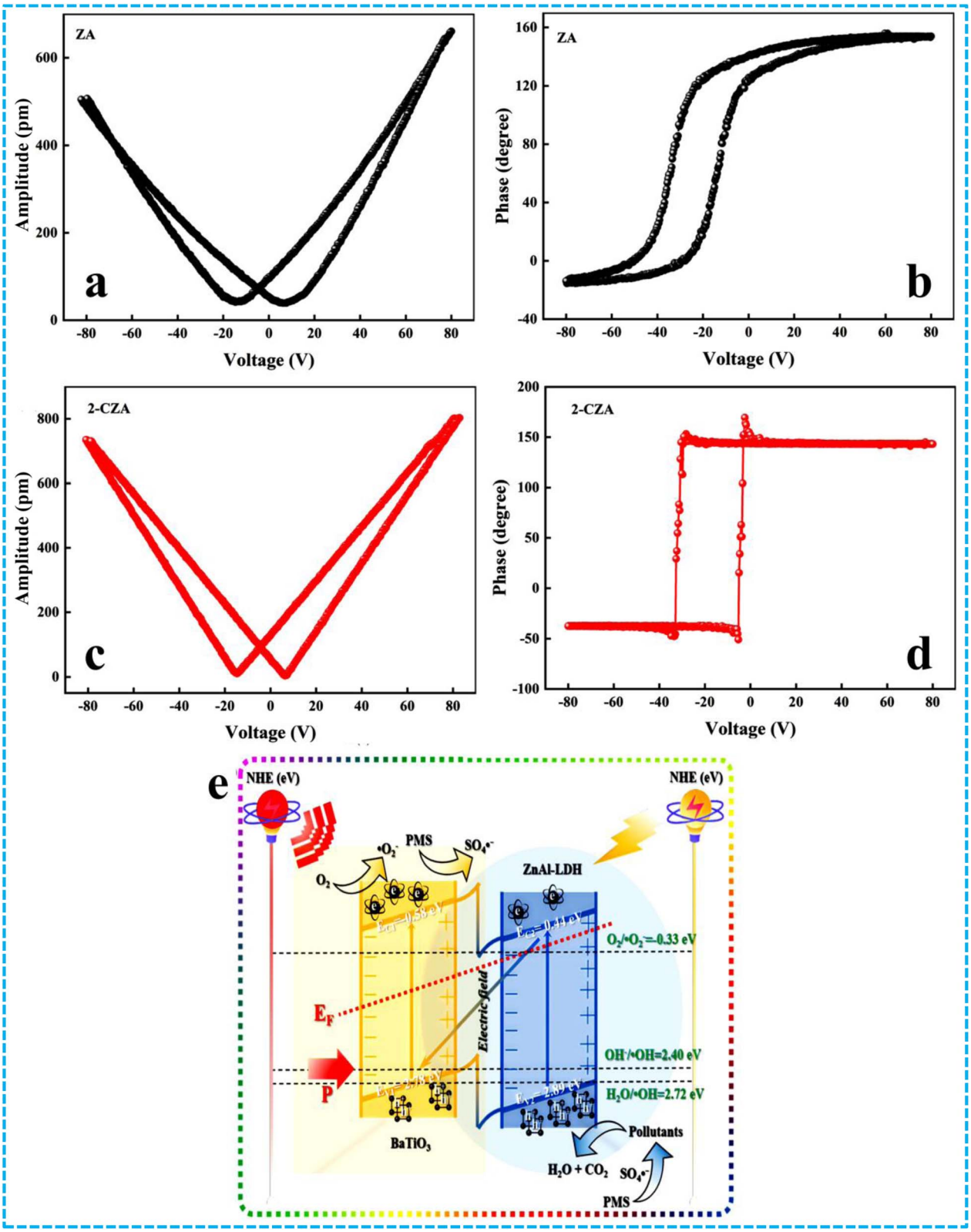

Fig. 16 PFM amplitude–voltage butterfly loops of (a) ZA and (c) 2-CZA and the corresponding phase–voltage hysteresis loops of (b) ZA and (d) 2-CZA, reproduced with permission from Elsevier. Copyright © 2023.[90] (e) Piezoelectric induced photocatalytic mechanism in $BaTiO_3$/ZnAl-LDH composites, reproduced with permission from Elsevier. Copyright © 2024.[91]

structure for transferring mechanical energy into electrical stimulation, and flexibility in ion-exchangeable capacity, which enhances interlayer polarization for deformation, and maintain stable phase and morphology under ultrasonication. Moreover, ZnAl-LDH are made up of stacked positively-charged layers with intercalated charge-compensating anions. When external strain is applied, the layer thickness, *i.e.*, odd-numbered layer, develops a polarization potential due to the lattice displacement, which causes excitons to accelerate in opposite directions, reducing charge recombination, for enhanced redox reactions.[38] Fascinated by the incredible properties of ZnAl-LDH, Y. Lu *et al.* fabricated Co-doped ZnAl-LDH (CZA) piezoelectric catalysts using a one-step hydrothermal method for PMS-based AOPs aimed at degrading norfloxacin. The CZA composite shows a degradation efficiency of 91.50% in 15 minutes, with a rate constant of 0.1644 min^{-1}. The higher effectiveness of CZA in NOR degradation emphasizes the key role of cobalt ions as the primary active sites, which are noteworthy for their ability to accelerate carrier transport while aiding the reconstruction of the catalytic active centre (Co^{2+}). Furthermore, the atomic and interfacial structure arrangement introduces defect levels caused by numerous localized states created by cobalt doping, which benefits the charge transfer rate. The piezoelectric properties of the CZA catalyst surface were explored using piezo-response force microscopy (PFM), showing butterfly-like amplitude loops as depicted in Fig. 16a–d and the phase lag loop with 180° polarization under a reversal voltage of ±80 V, which validates the substantial piezoelectric properties of ZA and 2-CZA catalysts. As compared to ZA, the 2-CZA showed greater distortion amplitude and phase lag loop area, suggesting the superior piezoelectric properties of 2-CZA, to generate substantial piezoelectric polarization for improved carrier transfer efficacy.[90] Owing to the remarkable structural adaptability and piezoelectric qualities of ZnAl-LDH, Zheng *et al.* developed $BaTiO_3$/ZnAl-LDH hybrid with dual piezoelectric properties. The composite materials synthesized through self-assembly and hydrothermal methods, which revealed excellent piezoelectric characteristics. Under ultrasonic vibration and sunlight, these composites showcased superior piezoelectric photocatalytic capabilities, achieving 99% NTP and 100% TC degradation within 45 min. The remarkable activity of the $BaTiO_3$/ZnAl-LDH composite is due to polarized

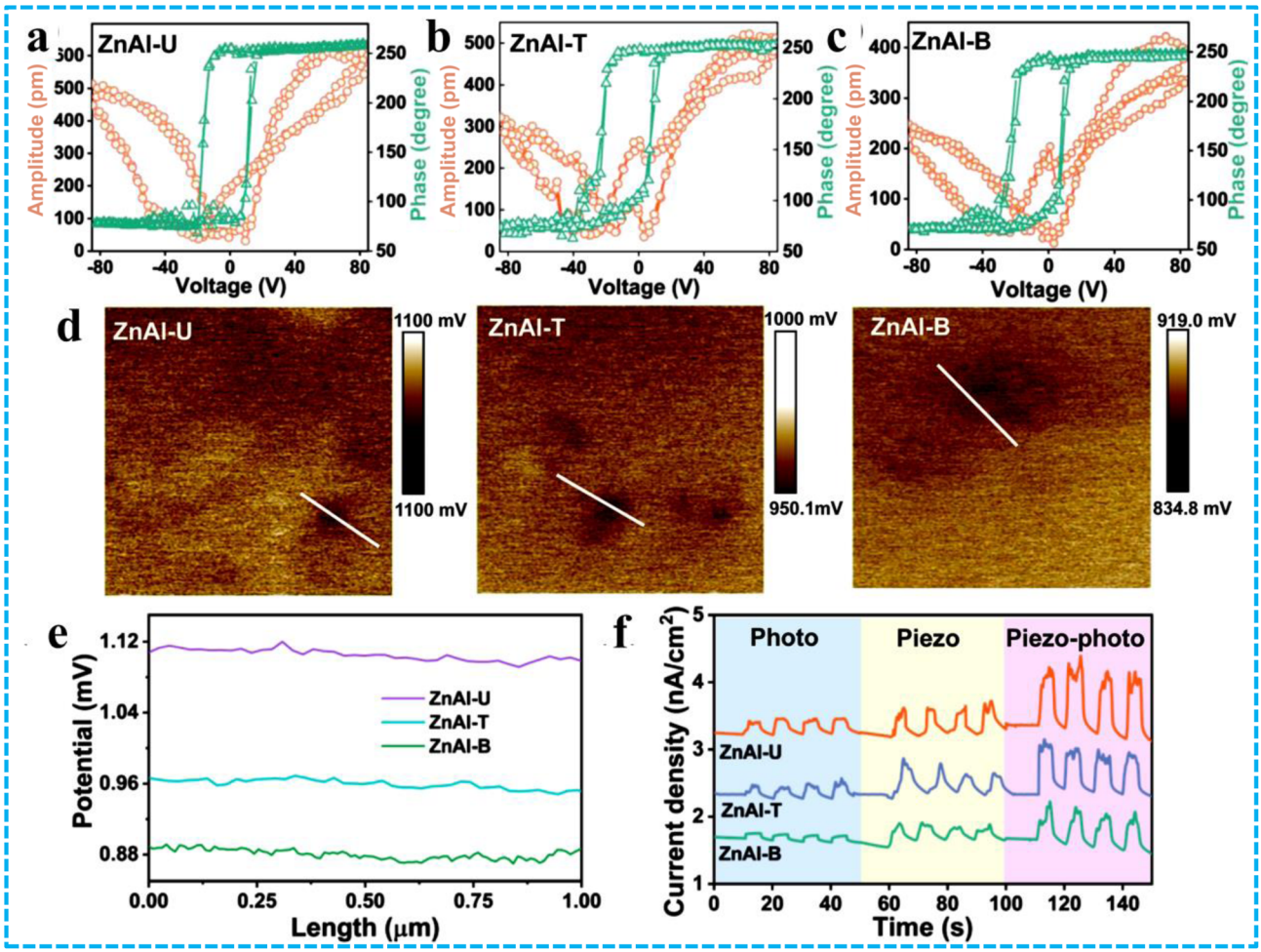

Fig. 17 (a–c) PFM butterfly loops and hysteresis loops of ZnAl-LDHs. (d) KPFM images and (e) the corresponding surface potential plot of ZnAl-LDH. (f) Transient current response of ZnAl-LDHs under various external irradiations, reproduced with permission from Elsevier. Copyright © 2022.[38]

Table 3 ZnAl-LDH-mediated systems for different photocatalytic applications

S. no.	Modified ZnAl-LDH systems	Synthesis method	Application	Reaction condition	Catalyst performance	Ref.
Doping						
1	Ce-doped ZnAl multi-metal oxide	Co-precipitation	Photodegradation of nitenpyram	Xenon lamp (300 W, 780 nm > λ > 420 nm), (50 mg L^{-1}) solution at 25 °C, stirred for 30 min under dark	50 mg L^{-1} of (NTP, 50 mL) removed in 60 min	93
2	Au-loaded ZnAl-LDH	Calcination–reconstruction	CH_4 photoconversion	—	(8504 μmol g^{-1} h^{-1}) with selectivity (92%)	94
3	Ag-loaded ZnAl-LDH	Mechanochemical	Methyl orange photodegradation	ZrO_2 balls of diameter 15 mm, rotation at 600 rpm for 2 h	95% degradation of MO in 180 min	95
4	Cu-doped ZnAl LDH	Urea hydrolysis and coprecipitation-conformation	Methylene blue photodegradation	150 W of xenon-arc lamp, nanocomposites (0.01 g), 24 h at the pH (6.5), 0.1 mL 1.5% of (H_2O_2)	96.98% photodegradation of MB after 360 min	96
5	Fullerene (C_{60})-doped Zn–Al LDH	Coprecipitation method	4-Chlorophenol photodegradation	Nanocomposites (0.01 g), 10 mL of 10 ppm of MB, a 150 W of xenon-arc lamp	95%, degradation after 5 h	53
6	Mn-doped Zn/Al LDH	Calcining and reconstructing routes	Photocatalytic NO removal	Stirring for 24 h at room temperature	99% degradation of 4-chlorophenol after 3 h	36
7	Ru monoatomic/ZnAl-LDH	Charge-attracting synthesis	Photocatalytic TCH degradation	Xenon lamp with a 420 nm filter, catalyst (10 mg)	100% degradation after 35 min	75
8	Bi doped ZnAl-LDH	Hydrothermal method	CIP photodegradation	300 W xenon lamp	97% degradation of the phenol	54
9	Halogen doped g-C_3N_4/ZnAl-LDH	*In situ* nucleation	Photodegradation of methyl orange (MO)	—	99.98% degradation after 40 min	52
10	Pt modified ZnAl-LDH	Co-precipitation	Phenol photodegradation	200 mg catalyst, 500 W Xe lamp, λ_{420}-cutoff filter	65–92% degradation in 90 min	60
11	Co doped ZnAl-LDH	One-step hydrothermal	Norfloxacin photodegradation	300 rpm stirring speed	Degradation efficiency of 91.50% within 15 min with rate constant of 0.1644 min^{-1}	90
Composite formation						
12	Ag_2O/Ag decorated ZnAl-LDH	Precipitation and thermal decomposition	TCH photodegradation	300 W Xe lamp with a 420 nm cutoff filter, 50 mg photocatalyst	(65–92% for 90 min)	97
13	ZnS/ZnAl-LDH	Hydrothermal method	Photocatalytic HER	UV and visible light. Stirred for 30 min in dark	633.58 μmol g^{-1} within 8 h	98
14	Bi_2MoO_6/Zn–Al (LDH)	Mechanochemical	Methylene blue photodegradation	400 W metal halide lamp, 0.05 g of the photocatalyst, 50 mL of RhB solution	99% of RhB in 80 min	51
15	Bi_2S_3/Zn–Al LDH	Electrostatic self-assembly	Methylene blue photodegradation	0.1 g of photocatalysts, 500 W xenon lamp, 5 mg of MB	99% of MB was degraded in 80 min	59

Table 3 (*Contd.*)

S. no.	Modified ZnAl-LDH systems	Synthesis method	Application	Reaction condition	Catalyst performance	Ref.
16	$ZnCdS/Bi_2WO_6$/ZnAl-LDH	Solvothermal	Photocatalytic HER	Mercury lamp (UV pen-ray), ($\lambda = 254$ nm), 100 mg of catalyst, 200 mL of a methanol–water solution (1 : 1, vol)	1599 mmol h^{-1}	79
17	(BPNs) ZnAl-(LDH)	Electrostatic self-assembly	MB photodegradation	300 W xenon lamp, 420 nm cut-off filter, 50 mg photocatalysts	99% of MB was degraded in 80 min	64
18	Fe_3O_4–ZnAl-LDH and TiO_2 composites	Sol–gel	Cr(VI) photoreduction	—	97% reduction after UV irradiation	99
19	Zn–Al LDH@g-C_3N_4@PDA/GO	Microwave irradiation	Ciprofloxacin photodegradation	35 W Xe arc lamp	84.10% degradation	100
20	SnO_2–ZnAl LDH	Co-precipitation	Rhodamine B photodegradation	600 rpm for 2 h	65% after 300 min	101
21	MoO_3/Zn–Al LDHs composite	Mechanochemical	Ciprofloxacin photodegradation	Xe lamp 500 W	Degradation 95%, after 5 h	45
22	ZnAl-LDH/MOF-5	Coprecipitation	CO_2 photoreduction	25 mg nanocomposite, at 6.5, oxidant H_2O_2	9.03 μmol g^{-1} h^{-1}	39
23	ZnAl-LDH@ZIF-8	Mechanochemical	Rhodamine B photodegradation	—	94% RHB degraded in 180 min	102
24	In_2S_3/Zn–Al LDHs	One-pot hydrothermal	TCH photodegradation	300 W xenon lamp, visible-light irradiation ($\lambda > 400$ nm), stirring for 30 min	92.2% degradation after 30 min	55
25	Graphdiyne (C_nH_{2n-2}) based CuI-GDY/ZnAl LDH	Solvothermal synthesis	Photocatalytic HER	ZACGDY (10 mg) and eosin Y (10 mg)	—	103
26	Fe_3O_4–SiO_2-EN@ZnAl-LDH	Sol–gel	CIP photodegradation	40 W, Hg vapor lamp as light source, 0.1–0.8 g L^{-1} photocatalyst, irradiation duration (0–60 min)	81.4% degradation	80
27	$ZnIn_2S_4$/ZnAl-LDH	Mechanochemical	SIPX xanthate photodegradation	Xenon lamp as light source, ($\lambda \geq 420$ nm), 20 mg photocatalyst, stirring at 500 rpm	95% degradation	83
28	$BaTiO_3$/ZnAl-LDH	Self-assembly and hydrothermal	Piezoelectric photocatalytic degradation of NTP and TC	Xenon lamp ($\lambda \geq 420$ nm)	Degradation of 99% for NTP and 100% TC within 45 minutes	91
Derived ZnAl-LDH-based heterostructures						
29	Calcined and organo-modified Zn–Al LDH	Calcination	Organic pollutants removal (acid red)	0.01 g composite photocatalyst, 165 min with a 70 W light source	Removal of acid red 14 in 165 min, >90	104

Table 3 (*Contd.*)

S. no.	Modified ZnAl-LDH systems	Synthesis method	Application	Reaction condition	Catalyst performance	Ref.
30	ZnS–ZnO/ZnAl-LDH	Calcination	RhB and paracetamol degradation	750 °C, simulated solar light, 240 min	97.8% degradation of RhB and 98.9% degradation of paracetamol after 240 min	105
31	$Ag/Ag_3PO_4/Zn–Al$ LDH	*In situ* co-precipitation *via* calcination	Removal of cationic dye (MB)	Xenon lamp (300 W, 780 nm > λ > 420 nm), 50 mL NTP (50 mg L^{-1}) solution at 25 °C	Degradation of aqueous 2 × 10^{-5} M MB	63
32	$NiFe_2O_4$–ZnAl-MMO	Hydrothermal *via* calcination	MO degradation	0.16 g of catalyst, UV-vis light source ($\lambda \geq 420$ nm), 1 h under magnetic stirring	95% degradation of MO under in 180 min	62
33	Ag–ZnO–Al_2O_3 heterostructure	Solid-state process	MO degradation	UV mercury lamp (400 W), 50 mg L^{-1} of catalyst	95.8% degradation of MO degradation after 210 min	85
34	ZnAl-LDH/GO composite	Wet chemical decomposition	Methylene blue (MB) degradation and Cr(VI) reduction	Natural sunlight, 50 mL of 15 mg L^{-1} of Cr(VI) solution and 50 mg L^{-1} of solid catalysts	—	61
35	ZnAl LDH-derived sulfides	Topological vulcanization	HER and tetracycline degradation	300 W xenon lamp, 10 mg of photocatalysts	H_2 production rate (11.89 mmol g^{-1} h^{-1}) and (91.94%) tetracycline degradation	86
36	Ultrathin ZnO/Al_2O_3 composite	Calcination and ultrasonication	Piezo catalytic methyl orange degradation	10 mg of sample, ultrasonic cleaner with frequency (~40 kHz and power of 100 W)	100% decolorization of MO within 15 min	92
Intercalated ZnAl-LDH systems						
37	MoS_2 intercalated ZnAl-LDH	*In situ* growth	Water splitting and organic pollutant degradation	300 W xenon lamp	After 60 min removal efficiency 63.12% and 93.12%	56
38	ZnS QD intercalated ZnAl-LDH	Hydrothermal	Water splitting and organic pollutant degradation	—	—	37
39	Anions modulated ZnAl-LDH	Modified coprecipitation	Photocatalytic CO_2 reduction	25 mg of the photocatalyst, Xe lamp as light source, vacuumed for 30 min	CO production rate of 3.80 μmol g^{-1} h^{-1}	89

electric fields induced by ultrasonic vibration within the ZnAl-LDH and $BaTiO_3$ components, and retention of the inherent electric field intensity across the heterojunction interfaces facilitates the movement of photoinduced carriers (Fig. 16e). This, in turn, improves carrier separation efficiency and creates a coupled catalytic response using dual piezoelectricity when exposed to visible light. This research highlights the potential of piezoelectric photocatalysis for effective pollutant removal, suggesting its use in municipal wastewater treatment and sterilization, as well as providing new insights for advancing piezoelectric photocatalyst development.[91]

Ultrathin ZnAl-LDH, only a few atoms thick, shows unique physicochemical properties with high mechanical strength and flexibility due to illumination of edge and surface-active sites. In this particular concept, J. Hu *et al.* reported piezo-photocatalytic behaviour of thickness-oriented ZnAl-LDHs synthesized by a one-step hydrothermal method towards carbamazepine (CBZ) degradation. The extremely thin ZnAl-LDH sheets (ZnAl-U) displayed 95.8% piezo-photocatalytic efficiency with a reaction rate constant of 0.148 min^{-1} for CBZ degradation, which is 1.61 and 3.02 times greater than thin ZnAl-LDH (ZnAl-T) and bulk ZnAl-LDH (ZnAl-B), respectively. The more rapid distortion of the thinner layer of ZnAl-U by mechanical stress generates piezoelectric polarization, thereby offering an optimal force for accelerating the separation of photo-generated charge pairs, resulting in a larger piezo photocurrent intensity (Fig. 17a–c). Furthermore, the energy band shifting induced by the piezoelectric potential due to combined ultrasonic and light irradiation segregates the photogenerated e^- and h^+ and promotes ROS for increased photocatalytic redox activity, which is supported by EPR and transient current response. Additionally, to further correlate the catalyst thickness and the piezoelectric strength, Kelvin probe force microscopy (KPFM) measurements of various catalyst thicknesses were evaluated. The highest surface potentials under probing stress for ZnAl-U, ZnAl-T, and ZnAl-B are 1.12, 0.96, and 0.88 mV, respectively (Fig. 17d), revealing a decrease pattern with thickness. The on–off photocurrent in piezocatalytic, photocatalytic, and piezo-photocatalytic processes are also varied with the thickness of ZnAl-LDHs, following the trend as: ZnAl-U > ZnAl-T > ZnAl-B, consistent with PFM and KPFM outcomes. Accordingly, stronger piezoelectric potential is produced by thinner layers, such as ZnAl-U, which improves charge separation. This is because the thinnest ZnAl-U layers deformed more easily, creating stronger piezoelectric potentials for enhanced charge separation as evident in Fig. 17e and f. Interestingly, the current intensity of piezo-photocatalytic exceeds that of piezo-catalytic and photocatalytic process, confirming the improved photogenerated charges separation by the piezoelectric field.[38] Later, Q. Nie *et al.* synthesized an ultrathin ZnO/Al_2O_3 (U-ZnO/Al_2O_3) composite by calcining a ZnAl-LDH precursor. The resulting ZnO/Al_2O_3 composite, shows a facile piezo-catalytic reaction rate for methyl orange dye degradation due to its ability to undergo easy bending deformation through mechanical forces. The production of ultrathin ZnO nanosheets, employing defect sites (O_V), raised the surface charge density near the valence band maximum and facilitated the build-up of a large concentration of charge carriers, leading to a greater piezoelectric potential on lateral surfaces (1.42 V) for piezocatalytic processes. Additionally, localized electrons around defect sites create a new intermediate band state that overlaps with the valence band of ZnO (mainly O 2p), narrowing the band gap and improving the charge mobility and conductivity. This phenomenon allows more electrons to be excited and separated by the generated piezoelectric potential, resulting in the formation of radical species like hydroxyl radicals for effective degradation. A comparative table of the ZnAl-LDH-mediated systems for different photocatalytic applications has been presented in Table 3.[92]

6. Summary

In summary, we have effectively explored the design and progress of ZnAl-LDH-based high-performance materials as potential photocatalysts, for green energy production and environmental applications, and piezo-polarized induced photocatalytic environmental applications. These comprised photocatalytic H_2 evolution, CO_2 reduction, and pollutant degradation, along with piezo-polarized pollutant degradation. Therefore, intending to offer the source of the photocatalytic achievement for extremely efficient ZnAl-LDH-based high-performance catalysts, this review precedes the recent advancement in the strategic modification for enhancing the photocatalytic performance of ZnAl-LDH, and the mechanistic pathway for providing the origin of the augmented photocatalytic activities of modified ZnAl-LDH-based photocatalysts. By manipulating the metal cation dopants, variation of the intercalated anions, adaptability of the structure, and execution of the heterostructure formation, ZnAl-LDH-based high-performance catalysts with improved complementary benefits and elevated photocatalytic activities were designed and fabricated. The design process of ZnAl-LDH-based high-performance catalysts, including co-precipitation, hydrothermal, and calcination methods, deliberately impacts their structural and electronic properties. The modified ZnAl-LDH-based catalysts were executed using the concepts of photocatalysis for effective light absorption, charge separation, and migration over the catalyst surface for the redox reaction of reactants to produce the desired products. Furthermore, mechanistic understanding discloses that the pairing of photocatalytic and piezoelectric effects advances the separation of carrier charge pairs for effective excitonic transfer triggered by the surface charge alteration and carrier charge separation at the bulk and interfacial area.[106,107]

7. Challenges and future perspective

After going through the above literatures, even with these noteworthy achievements, certain constraints still need to be overcome to improve the catalytic efficiency of ZnAl-LDH-based material in real-time implementation. The subsequent several aspects must be taken into consideration:

(i) Optimization of charge transport dynamics and reaction mechanism of ZnAl-LDH-based materials remains subtle, such

as the influence of the structural and electronic properties on the photocatalytic activity and stability of the modified photocatalysts. Therefore, advanced theoretical modelling and *in situ* characterization techniques should be implemented to understand the carrier charge dynamics. For example, *in situ* Raman spectroscopy studies could provide key information about the presence of surface defect sites, together with their transformational paths. Alternatively, *in situ* XRD could afford relevant data on the dynamic modification of the structure of an evolving photocatalyst under a change in reaction conditions. In the meantime, DFT computational studies are crucial for providing insights into the kinetics of chemically active centres and reaction mechanisms in heterogeneous reactions, by envisaging the reaction intermediates and transition states, during the entire course of the reaction. They necessitate distinct characterization and verification techniques. Also, the hybrid structure formation with other 2D materials such as graphene, MXenes, *etc.*, could be further explored for improved charge separation efficiency to attain maximum efficiency.

(ii) The long-term material stability under practical applications must be taken forward *via* material modification and composite formation using an advanced design process. Studies reveal that recyclable commercial catalysts in the pilot scale for industrial applications are still lacking. Therefore, scalable and low-cost synthesis processes should be developed for ZnAl-LDH-based photocatalysts for industrial applications. For example, ZnAl-LDH-in combination with magnetic material could act as a highly efficient recyclable catalyst for practical applications. Furthermore, fixed-bed photoreactors should be executed on a pilot scale for better efficiency measurement.

(iii) The combination of piezoelectric properties of the material with photoactivity improves the carrier charge separation process and extends the light absorption behaviour of this material under mechanical stress. Though piezo-polarized photocatalytic pollutant degradation has recently made phenomenal progress using ZnAl-LDH-based material by thickness adjustment, the technology is still in its initial stages. Additionally, a better understanding of the fundamental factors influencing wide band gap tuning, and generation of induced piezo by coupling ZnAl-LDH-based material with piezo active materials is required to be explored for achieving high material efficiency.

(iv) The intrinsic complexity of ZnAl-LDH nanostructures, especially their layered architectures and interlayer interactions, poses significant challenges for precise morphological control. Tailoring it into quantum dots, monolayers, or hierarchical nanostructures remains difficult due to their rigid brucite-like layers and strong hydrogen bonding, which complicate structural transformation and downscaling to lower dimensions such as 0D quantum dots or 1D arrays. In this context, advances in hydrothermal, solvothermal, and exfoliation techniques are enabling the controlled synthesis of ZnAl-LDH with diverse morphologies—from nanosheets to hierarchical superstructures. Such designs enhance surface area, expose active sites, and reduce charge diffusion distances, making it more suitable for water splitting and CO_2 reduction.

Author contributions

Naisargika Mallick: conceptualization, visualization, writing – original draft, scheme designing; Susanginee Nayak: conceptualization, visualization, writing – original draft, writing – reviewing and editing, supervision; Anshumika Mishra: writing – original draft, writing – reviewing and editing, scheme designing; Upali Aparajita Mohanty: writing – reviewing and editing, scheme designing; Kulamani Parida: conceptualization, visualization, writing – reviewing and editing, supervision.

Conflicts of interest

There are no conflicts to declare.

Data availability

The data used to support the findings of the study are within the article.

Acknowledgements

The authors are thankful to the management of Siksha 'O' Anusandhan Deemed to be University for the financial support for the research work. The author, Dr Susanginee Nayak, expresses profound acknowledgment to the Council of Scientific and Industrial Research (CSIR)-India for awarding the CSIR-Research Associateship (RA)-CSIR-RA fellowship for financial assistance vide file no. 09/969 (0011)/2020 EMR-1. Upali Aparajita Mohanty is grateful to UGC for the award of a SJSGC fellowship (UGCES-22-GE-ORI-FSJSGC-5637).

References

1 Y. Wang, M. Zhang, Y. Liu, Z. Zheng, B. Liu, M. Chen, G. Guan and K. Yan, Recent advances on transition-metal-based layered double hydroxides nanosheets for electrocatalytic energy conversion, *Adv. Sci.*, 2023, **10**, 2207519.

2 M. Sajid and I. Ihsanullah, Magnetic layered double hydroxide-based composites as sustainable adsorbent materials for water treatment applications: Progress, challenges, and outlook, *Sci. Total Environ.*, 2023, **880**, 163299.

3 Z. Z. Yang, J. J. Wei, G. M. Zeng, H. Q. Zhang, X. F. Tan, C. Ma, X. C. Li, Z. H. Li and C. Zhang, A review on strategies to LDH-based materials to improve adsorption capacity and photoreduction efficiency for CO_2, *Coord. Chem. Rev.*, 2019, **386**, 154–182.

4 M. Xie, C. Liu, M. Liang, S. Rad, Z. Xu, S. You and D. Wang, A review of the degradation of antibiotic contaminants using advanced oxidation processes: modification and application of layered double hydroxides based materials, *Environ. Sci. Pollut. Res.*, 2024, **31**, 18362–18378.

5 E. M. Abd El-Monaem, H. M. Elshishini, S. S. Bakr, H. G. El-Aqapa, M. Hosny, G. Andaluri, G. M. El-Subruiti, A. M. Omer and A. S. Eltaweil, A comprehensive review on LDH-based

catalysts to activate persulfates for the degradation of organic pollutants, *npj Clean Water*, 2023, **6**, 34–57.

6 G. Ren, H. Han, Y. Wang, S. Liu, J. Zhao, X. Meng and Z. Li, Recent advances of photocatalytic application in water treatment: A review, *Nanomaterials*, 2021, **11**, 1804.

7 L. Biswal, S. Nayak and K. Parida, Recent progress on strategies for the preparation of 2D/2D MXene/g-C_3N_4 nanocomposites for photocatalytic energy and environmental applications, *Catal. Sci. Technol.*, 2021, **1**, 1222–1248.

8 A. Mishra, N. Priyadarshini, S. Mansingh and K. Parida, Recent advancement in $LaFeO_3$-mediated systems towards photocatalytic and photoelectrocatalytic hydrogen evolution reaction: A comprehensive review, *Adv. Colloid Interface Sci.*, 2024, **333**, 103300.

9 A. Mishra, N. Priyadarshini and K. Parida, Synergistic interplay between oxygen-vacancy and S-scheme charge transfer dynamics in an $LaFeO_3$/FeOOH heterojunction towards sono-assisted photo-Fenton antibiotic degradation and water splitting, *Inorg. Chem. Front.*, 2025, **12**, 5369–5388.

10 L. Acharya, G. Swain, B. P. Mishra, R. Acharya and K. Parida, Development of $MgIn_2S_4$ microflower-embedded exfoliated B-doped g-C_3N_4 nanosheets: p–n heterojunction photocatalysts toward photocatalytic water reduction and H_2O_2 production under visible-light irradiation, *ACS Appl. Energy Mater.*, 2022, **5**, 2838–2852.

11 K. K. Das, S. Mansingh, R. Mohanty, D. P. Sahoo, N. Priyadarshini and K. Parida, 0D–2D Fe_2O_3/boron-doped g-C_3N_4 S-scheme exciton engineering for photocatalytic H_2O_2 production and photo-fenton recalcitrant-pollutant detoxification: kinetics, influencing factors, and mechanism, *J. Phys. Chem. C*, 2022, **127**, 22–40.

12 L. Biswal, B. P. Mishra, S. Das, L. Acharya, S. Nayak and K. Parida, Nanoarchitecture of a Ti_3C_2@TiO_2 hybrid for photocatalytic antibiotic degradation and hydrogen evolution: stability, kinetics, and mechanistic insights, *Inorg. Chem.*, 2023, **62**, 7584–7597.

13 R. Acharya and K. Parida, A review on TiO_2/g-C_3N_4 visible-light-responsive photocatalysts for sustainable energy generation and environmental remediation, *J. Environ. Chem. Eng.*, 2020, **8**, 103896.

14 D. Kandi, S. Mansingh, A. Behera and K. Parida, Calculation of relative fluorescence quantum yield and Urbach energy of colloidal CdS QDs in various easily accessible solvents, *J. Lumin.*, 2021, **231**, 117792.

15 S. P. Tripathy, S. Subudhi, A. Ray, P. Behera, A. Bhaumik and K. Parida, Mixed-valence bimetallic Ce/Zr MOF-based nanoarchitecture: a visible-light-active photocatalyst for ciprofloxacin degradation and hydrogen evolution, *Langmuir*, 2022, **38**, 1766–1780.

16 S. Subudhi, S. P. Tripathy and K. Parida, Highlights of the characterization techniques on inorganic, organic (COF) and hybrid (MOF) photocatalytic semiconductors, *Catal. Sci. Technol.*, 2021, **11**, 392–415.

17 H. Boumeriame, E. S. Da Silva, A. S. Cherevan, T. Chafik, J. L. Faria and D. Eder, Layered double hydroxide (LDH)-based materials: A mini-review on strategies to improve the performance for photocatalytic water splitting, *J. Energy Chem.*, 2022, **64**, 406–431.

18 A. Ali Khan and M. Tahir, Constructing S-scheme heterojunction of CoAlLa-LDH/g-C_3N_4 through monolayer Ti_3C_2-MXene to promote photocatalytic CO_2 re-forming of methane to solar fuels, *ACS Appl. Energy Mater.*, 2021, **5**, 784–806.

19 L. Wang, Z. Zhu, F. Wang, Y. Qi, W. Zhang and C. Wang, State-of-the-art and prospects of Zn-containing layered double hydroxides (Zn-LDH)-based materials for photocatalytic water remediation, *Chemosphere*, 2021, **278**, 130367.

20 A. Sherryna and M. Tahir, Recent developments in layered double hydroxide structures with their role in promoting photocatalytic hydrogen production: A comprehensive review, *Int. J. Energy Res.*, 2022, **46**, 2093–2140.

21 Z. Liu, M. A. Nazir, M. Altaf, H. Majeed, Z. M. El-Bahy, M. H. Helal, A. Rauf, S. Ullah, T. Najam, S. S. Shah and A. ur Rehman, Light-driven C1 Chemical Conversion with LDH-based Nanomaterials, *Appl. Clay Sci.*, 2024, **258**, 107488.

22 M. J. Wu, J. Z. Wu, J. Zhang, H. Chen, J. Z. Zhou, G. R. Qian, Z. P. Xu, Z. Du and Q. L. Rao, A review on fabricating heterostructures from layered double hydroxides for enhanced photocatalytic activities, *Catal. Sci. Technol.*, 2018, **8**, 1207–1228.

23 S. Nayak, G. Swain and K. Parida, Enhanced Photocatalytic Activities of RhB Degradation and H_2 Evolution from in Situ Formation of the Electrostatic Heterostructure MoS_2/NiFe LDH Nanocomposite through the Z-Scheme Mechanism via p–n Heterojunctions, *ACS Appl. Mater. Interfaces*, 2019, **11**, 20923–20942.

24 P. Bobde, A. K. Sharma, D. Panchal, A. Sharma, R. K. Patel, R. S. Dhodapkar and S. Pal, Layered double hydroxides (LDHs)-based photocatalysts for dye degradation: A review, *Int. J. Environ. Sci. Technol.*, 2023, **20**, 5733–5752.

25 B. Song, Z. Zeng, G. Zeng, J. Gong, R. Xiao, S. Ye, M. Chen, C. Lai, P. Xu and X. Tang, Powerful combination of g-C_3N_4 and LDHs for enhanced photocatalytic performance: a review of strategy, synthesis, and applications, *Adv. Colloid Interface Sci.*, 2019, **272**, 101999.

26 G. Zhang, X. Zhang, Y. Meng, G. Pan, Z. Ni and S. Xia, Layered double hydroxides-based photocatalysts and visible-light driven photodegradation of organic pollutants: A review, *Chem. Eng. J.*, 2020, **392**, 123684.

27 M. J. Wu, J. Z. Wu, J. Zhang, H. Chen, J. Z. Zhou, G. R. Qian, Z. P. Xu, Z. Du and Q. L. Rao, A review on fabricating heterostructures from layered double hydroxides for enhanced photocatalytic activities, *Catal. Sci. Technol.*, 2018, **8**, 1207–1228.

28 P. Shandilya, R. Sharma, R. K. Arya, A. Kumar, D. V. Vo and G. Sharma, Recent progress and challenges in photocatalytic water splitting using layered double hydroxides (LDH) based nanocomposites, *Int. J. Hydrogen Energy*, 2022, **47**, 37438–37475.

29 G. Zhao, J. Zou, X. Chen, J. Yu and F. Jiao, Layered double hydroxides materials for photo (electro-) catalytic applications, *Chem. Eng. J.*, 2020, **397**, 125407.
30 S. Nayak and K. Parida, Superactive NiFe-LDH/graphene nanocomposites as competent catalysts for water splitting reactions, *Inorg. Chem. Front.*, 2020, **7**, 3805–3836.
31 L. Mohapatra and K. Parida, A review on the recent progress, challenges and perspective of layered double hydroxides as promising photocatalysts, *J. Mater. Chem. A*, 2016, **4**, 10744–10766.
32 D. P. Sahoo, K. K. Das, S. Mansingh, S. Sultana and K. Parida, Recent progress in first row transition metal Layered double hydroxide (LDH) based electrocatalysts towards water splitting: A review with insights on synthesis, *Coord. Chem. Rev.*, 2022, **469**, 214666.
33 Á. Patzkó, R. Kun, V. Hornok, I. Dékány, T. Engelhardt and N. Schall, ZnAl-layer double hydroxides as photocatalysts for oxidation of phenol in aqueous solution, *Colloids Surf., A*, 2005, **265**, 64–72.
34 H. Wang, X. Xiang and F. Li, Hybrid ZnAl-LDH/CNTs nanocomposites: Noncovalent assembly and enhanced photodegradation performance, *AIChE J.*, 2010, **56**, 768–778.
35 F. Tzompantzi, A. Mantilla, F. Bañuelos, J. L. Fernández and R. Gómez, Improved photocatalytic degradation of phenolic compounds with ZnAl mixed oxides obtained from LDH materials, *Top. Catal.*, 2011, **54**, 257–263.
36 G. Morales-Mendoza, F. Tzompantzi, C. García-Mendoza, R. López, V. De la Luz, S. W. Lee, T. H. Kim, L. M. Torres-Martinez and R. Gomez, Mn-doped Zn/Al layered double hydroxides as photocatalysts for the 4-chlorophenol photodegradation, *Appl. Clay Sci.*, 2015, **118**, 38–47.
37 A. R. Amani-Ghadim, F. Khodam and M. S. Dorraji, ZnS quantum dot intercalated layered double hydroxide semiconductors for solar water splitting and organic pollutant degradation, *J. Mater. Chem. A*, 2019, **7**, 11408–11422.
38 J. Hu, C. Yu, C. Li, S. Lan, L. Zeng and M. Zhu, Thickness-dependent piezo-photo-responsive behavior of ZnAl-layered double hydroxide for wastewater remediation, *Nano Energy*, 2022, **101**, 107583–107592.
39 A. Chakraborty and H. Acharya, ZnAl–LDH/MOF-5 heterostructure nanocomposite for photocatalytic degradation of organic dyes under sunlight irradiation, *New J. Chem.*, 2023, **47**, 1498–1507.
40 J. Zheng, C. Fan, X. Li, Q. Yang, D. Wang, A. Duan and S. Pan, Tourmaline/ZnAL-LDH nanocomposite based photocatalytic system for efficient degradation of mixed pollutant wastewater, *Sep. Purif. Technol.*, 2024, **345**, 127306.
41 J. Yang, Y. Zhang, K. Wei, Y. Xue, L. Cai, H. Han, C. Ma and S. Feng, ZnAl-LDH nanosheets/$Bi_{24}O_{31}Br_{10}$ S-scheme heterojunction toward boosted photocatalytic CO_2 reduction, *Sep. Purif. Technol.*, 2025, 134494.
42 U. A. Mohanty, D. P. Sahoo, K. K. Das, L. Paramanik and K. Parida, Facilitated visible-light-driven peroxymonosulfate activation by a Co–Fe layered double hydroxide derived p–n heterostructure for sulfadiazine degradation: affecting parameters, kinetics, and mechanistic insights, *Inorg. Chem.*, 2024, **63**, 1919–1937.
43 P. Prabha Sarangi, D. Prava Sahoo, U. Aparajita Mohanty, S. Nayak and K. Parida, Recent advancement in quantum dot modified layered double hydroxide towards photocatalytic, electrocatalytic, and photoelectrochemical applications, *ChemCatChem*, 2024, **16**, 202301533.
44 P. Veisi, M. S. S. Dorraji, M. H. Rasoulifard, S. Ghaffari and A. K. Choobar, Synergistic photocatalytic-adsorption removal effect of $NiFe_2O_4$-Zn-Al mixed metal oxide composite under visible-light irradiation, *J. Photochem. Photobiol., A*, 2021, **414**, 113268.
45 J. Wang, X. Lei, C. Huang, L. Xue, W. Cheng and Q. Wu, Fabrication of a novel MoO_3/Zn–Al LDHs composite photocatalyst for efficient degradation of tetracycline under visible light irradiation, *J. Phys. Chem. Solids*, 2021, **148**, 109698.
46 M. V. Bukhtiyarova, A review on effect of synthesis conditions on the formation of layered double hydroxides, *J. Solid State Chem.*, 2019, **269**, 494–506.
47 A. A. Khan, M. Tahir and N. Khan, LDH-based nanomaterials for photocatalytic applications: A comprehensive review on the role of bi/trivalent cations, anions, morphology, defect engineering, memory effect, and heterojunction formation, *J. Energy Chem.*, 2023, **84**, 242–276.
48 D. Xu, G. Fu, Z. Li, W. Zhen, H. Wang, M. Liu, J. Sun, J. Zhang and L. Yang, Functional regulation of ZnAl-LDHs and mechanism of photocatalytic reduction of CO_2: a DFT study, *Molecules*, 2023, **28**, 738–754.
49 G. Ding, Z. Wang, J. Zhang, P. Wang, L. Chen and G. Liao, Layered double hydroxides-based Z-scheme heterojunction for photocatalysis, *EcoEnergy*, 2024, **2**, 22–44.
50 D. Chaillot, S. Bennici and J. Brendlé, Layered double hydroxides and LDH-derived materials in chosen environmental applications: a review, *Environ. Sci. Pollut. Res.*, 2021, **28**, 24375–24405.
51 H. Li, Q. Deng, J. Liu, W. Hou, N. Du, R. Zhang and X. Tao, Synthesis, characterization and enhanced visible light photocatalytic activity of Bi_2MoO_6/Zn–Al layered double hydroxide hierarchical heterostructures, *Catal. Sci. Technol.*, 2014, **4**, 1028–1037.
52 J. Hu, C. Sun, L. X. Wu, G. Q. Zhao, H. Y. Liu and F. P. Jiao, Halogen doped g-C_3N_4/ZnAl-LDH hybrid as a Z-scheme photocatalyst for efficient degradation for tetracycline in seawater, *Sep. Purif. Technol.*, 2023, **309**, 123047.
53 O. O. Balayeva, T. S. Israfilli and A. A. Azizov, Fullerene (C_{60})-doped zinc-aluminium layered double hydroxide/polyvinyl alcohol nanocomposites: Synthesis, characterization, and photodegradation of methylene blue from water solution, *J. Chin. Chem. Soc.*, 2024, **71**, 21–34.
54 L. Wang, Z. Xiang, H. Zhang, Y. Deng, J. Wang, H. Xiao, W. Wang and X. Song, Bi-doped ZnAl-layered double hydroxides with enhanced photocatalytic activity for ciprofloxacin degradation: the synergistic effect of Bi

doping and oxygen vacancies, *New J. Chem.*, 2024, **48**, 5681–5695.

55 M. Wang, J. Wang, M. Li, X. Wang, Y. Sima and Q. Wu, Novel In_2S_3/Zn–Al LDHs composite as an efficient visible-light-driven photocatalyst for tetracycline degradation, *Opt. Mater.*, 2022, **128**, 112376.

56 S. Chen, F. Yang, Z. Cao, C. Yu, S. Wang and H. Zhong, Enhanced photocatalytic activity of molybdenum disulfide by compositing ZnAl–LDH, *Colloids Surf., A*, 2020, **586**, 124140.

57 T. Tsuzuki and P. G. McCormick, Mechanochemical synthesis of nanoparticles, *J. Mater. Sci.*, 2004, **39**, 5143–5146.

58 T. Ma, C. Liu, Z. Li, R. Zheng, M. Chen, S. Dai and T. Zhao, Mechanochemically constructed Bi_2WO_6/Zn-Al layered double hydroxide heterojunction with prominent visible light-driven photocatalytic efficiency, *Appl. Clay Sci.*, 2021, **215**, 106328.

59 Z. Li, Q. Zhang, X. Liu, M. Chen, L. Wu and Z. Ai, Mechanochemical synthesis of novel heterostructured Bi_2S_3/Zn-Al layered double hydroxide nano-particles as efficient visible light reactive Z-scheme photocatalysts, *Appl. Surf. Sci.*, 2018, **452**, 123–133.

60 Z. Li, M. Chen, H. Hu, Q. Zhang and D. Tao, Mechanochemical synthesis of novel Pt modified ZnAl-LDH for effective ciprofloxacin photodegradation, *J. Solid State Chem.*, 2020, **290**, 121594.

61 D. A. Islam, G. M. Choudhury and H. Acharya, Layered double hydroxide (LDH)-derived zinc oxide (ZnO) nanorod on exfoliated graphene oxide (GO) nanosheet for photocatalytic dye degradation and hexavalent chromium reduction, *J. Solid State Chem.*, 2024, **336**, 124776.

62 P. Veisi, M. S. Dorraji, M. H. Rasoulifard, S. Ghaffari and A. K. Choobar, Synergistic photocatalytic-adsorption removal effect of $NiFe_2O_4$-Zn-Al mixed metal oxide composite under visible-light irradiation, *J. Photochem. Photobiol.*, 2021, **414**, 113268.

63 J. Zheng, W. Li, R. Tang, S. Xiong, D. Gong, Y. Deng, Z. Zhou, L. Li, L. Su and L. Yang, Ultrafast photodegradation of nitenpyram by Ag/Ag_3PO_4/Zn–Al LDH composites activated by persulfate system: removal efficiency, degradation pathway and reaction mechanism, *Chemosphere*, 2022, **292**, 133431.

64 J. Yang, R. Jing, P. Wang, D. Liang, H. Huang, C. Xia, Q. Zhang, A. Liu, Z. Meng and Y. Liu, Black phosphorus nanosheets and ZnAl-LDH nanocomposite as environmental-friendly photocatalysts for the degradation of Methylene blue under visible light irradiation, *Appl. Clay Sci.*, 2021, **200**, 105902.

65 F. Mohamadpour and A. M. Amani, Photocatalytic systems: reactions, mechanism, and applications, *RSC Adv.*, 2024, **14**, 20609–20645.

66 D. Zhu and Q. Zhou, Action and mechanism of semiconductor photocatalysis on degradation of organic pollutants in water treatment: A review, *Environ. Nanotechnol., Monit. Manage.*, 2019, **12**, 100255.

67 E. Karamian and S. Sharifnia, On the general mechanism of photocatalytic reduction of CO_2, *J. CO_2 Util.*, 2016, **16**, 194–203.

68 J. Sun, Q. Hua, R. Zhou, D. Li, W. Guo, X. Li, G. Hu, C. Shan, Q. Meng, L. Dong and C. Pan, Piezo-phototronic effect enhanced efficient flexible perovskite solar cells, *ACS Nano*, 2019, **13**, 4507–4513.

69 R. Mohanty, S. Mansingh, K. Parida and K. Parida, Boosting sluggish photocatalytic hydrogen evolution through piezo-stimulated polarization: a critical review, *Mater. Horiz.*, 2022, **9**, 1332–1355.

70 S. Mansingh, N. Priyadarshini, J. Panda, K. K. Das, D. P. Sahoo, J. Sahu, D. Prusty, R. K. Giri, A. Mishra and K. Parida, Recent advancement in piezopolarization induced photocatalytic H_2O_2 production: fundamentals, theoretical insights, and future endeavors, *Energy Fuels*, 2024, **38**, 5632–5658.

71 A. Parija, K. K. Das, U. A. Mohanty and K. Parida, Multifunctional PVDF based composite for sustainable catalysis: Insights into piezo-photocatalytic environmental and energy application, *Chem. Eng. J.*, 2025, 167260.

72 J. Kang, S. Xue, C. Cheng, J. Qin, H. Li, A. J. Li, W. Guo, R. Yin and R. Qiu, Enhanced peroxydisulfate activation by photo-piezocatalysis based on zinc-aluminum layered double hydroxide for imidacloprid removal: Combined radical with nonradical pathways, *Sep. Purif. Technol.*, 2024, **345**, 127341.

73 E. Jiang, C. Guo, P. Huo, Y. Yan, P. Zhou and Y. Yan, Vertical growth of O-vacancy rich LDH atomic layers as OER-sensitive reactive sites to boost overall water splitting on perovskite oxides, *ACS Sustainable Chem. Eng.*, 2022, **10**, 16335–16343.

74 D. Li, L. Fan, Y. Shen, M. Qi, M. D. Ali, D. Liu and S. Li, Degradation of rhodamine B under visible-light by Cu-doped ZnAl layered double hydroxide, *J. Nanosci. Nanotechnol.*, 2019, **19**, 1090–1097.

75 J. Zheng, C. Fan, X. Li, Q. Yang, D. Wang, A. Duan, S. Pan and F. You, Intelligent multifunctional ruthenium monoatomic/ZnAl-LDH photocatalysts for simultaneous detection and rapid degradation of antibiotics, *J. Environ. Manage.*, 2024, **353**, 120156.

76 H. Yang, A short review on heterojunction photocatalysts: Carrier transfer behavior and photocatalytic mechanisms, *Mater. Res. Bull.*, 2021, **142**, 111406.

77 A. Balapure, J. R. Dutta and R. Ganesan, Recent advances in semiconductor heterojunctions: a detailed review of the fundamentals of photocatalysis, charge transfer mechanism and materials, *RSC Appl. Interfaces*, 2024, **1**, 43–69.

78 S. Kumar, A. Kumar, A. Kumar and V. Krishnan, Nanoscale zinc oxide based heterojunctions as visible light active photocatalysts for hydrogen energy and environmental remediation, *Catal. Rev.*, 2020, **62**, 346–405.

79 X. Sun, T. Hu, Y. Sun, X. Gao, Z. Cao, Y. Liu, L. Wang and L. Li, Flower-like spherical ZnCdS/Bi_2WO_6/ZnAl-LDH with dual type II heterostructure as a photocatalyst for efficient

photocatalytic degradation and hydrogen production, *J. Phys. Chem. Solids*, 2023, **183**, 111650.

80 T. J. Al-Musawi, P. pour Bahrami, R. Rahimpoor, N. Mengelizadeh and D. Balarak, Enhanced photocatalytic degradation of ciprofloxacin antibiotics using Fe_3O_4-SiO_2-EN@Zn-Al layered double hydroxide nanocomposites under the COVID-19 pandemic, *Results Eng.*, 2024, **24**, 103396.

81 M. Sun, Y. Liu, Y. Na, Z. Li, M. Chen, S. Dai, X. Guo, P. Li, T. Zhao and R. Zheng, Mechanochemical preparation of Z-scheme $CdIn_2S_4$/Zn-Al LDH heterojunction with enhanced photocatalytic performance for SIPX degradation, *J. Alloys Compd.*, 2025, **1010**, 177247.

82 Z. Zeng, X. Li, Q. Yang, D. Wang, A. Duan, S. Pan and J. Zheng, Ultrathin In_2O_3-Ov/ZnAl-LDH-Ov S-scheme heterojunctions with oxygen-rich vacancies for efficient photocatalytic peroxymonosulfate activation for the degradation of nitenpyram, *J. Environ. Chem. Eng.*, 2025, **13**, 115193.

83 M. Sun, Y. Mao, Y. Na, Y. Liu, Z. Li, M. Chen, P. Li, S. Dai and T. Zhao, Mechanochemical synthesis of novel Z-scheme $ZnIn_2S_4$/Zn–Al layered double hydroxides heterojunction with performed photodegradation of SIPX xanthate from aqueous solution, *Mater. Sci. Semicond. Process.*, 2024, **177**, 108406.

84 A. Gandamalla, S. Manchala, A. Verma, Y. P. Fu and V. Shanker, Microwave-assisted synthesis of ZnAl-LDH/g-C_3N_4 composite for degradation of antibiotic ciprofloxacin under visible-light illumination, *Chemosphere*, 2021, **283**, 131182.

85 F. Z. Janani, N. Taoufik, H. Khiar, A. Elhalil, S. Qourzal, M. Sadiq and N. Barka, Effect of Ag doping on photocatalytic activity of ZnO-Al_2O_3 derived from LDH structure: Synthesis, characterization and experimental study, *Appl. Surf. Sci. Adv.*, 2023, **16**, 100430.

86 J. Hu, S. A. Hussain, H. Liu, C. Hu and F. Jiao, Construction of ZnAl LDH-derived sulfides with etching modification to trigger photocatalytic H_2 production and degradation oxidation, *Inorg. Chem.*, 2024, **63**, 17238–17248.

87 J. Zhou, Z. Lin, H. Ren, X. Duan, I. Shakir, Y. Huang and X. Duan, Layered intercalation materials, *Adv. Mater.*, 2021, **33**, 2004557.

88 S. Su, X. Li, M. Tan, X. Zhang, Y. Wang, Y. Duan, J. Peng and M. Luo, Enhancement of the properties of ZnAl-LDHs for photocatalytic nitrogen reduction reaction by controlling anion intercalation, *Inorg. Chem. Front.*, 2023, **10**, 869–879.

89 Z. Hao, Z. Tian, X. Tian, L. Ma, Y. Gao, M. Shao and R. Zhang, Interlayer anions modulated ZnAl-layered double hydroxides for enhanced photocatalytic CO_2 reduction, *J. Alloys Compd.*, 2024, **995**, 174828.

90 Y. Lu, C. Ding, J. Guo, W. Gan, P. Chen, R. Chen, Q. Ling, M. Zhang, P. Wang and Z. Sun, Cobalt-doped ZnAl-LDH nanosheet arrays as recyclable piezo-catalysts for effective activation of peroxymonosulfate to degrade norfloxacin: non-radical pathways and theoretical calculation studies, *Nano Energy*, 2023, **112**, 108515.

91 J. Zheng, Z. Zeng, X. Li, Q. Yang, D. Wang, A. Duan and S. Pan, Barium titanate/ZnAl-layered double hydroxide catalysts for piezoelectrically enhanced photocatalytic degradation of coexisting pollutants and antibiotic resistance genes, *J. Environ. Chem. Eng.*, 2024, **12**, 114227.

92 Q. Nie, Y. Xie, J. Ma, J. Wang and G. Zhang, High piezocatalytic activity of ZnO/Al_2O_3 nanosheets utilizing ultrasonic energy for wastewater treatment, *Cleaner Prod. Lett.*, 2020, **242**, 118532.

93 J. Zhu, Z. Zhu, H. Zhang, H. Lu, Y. Qiu, L. Zhu and S. Küppers, Enhanced photocatalytic activity of Ce-doped Zn-Al multi-metal oxide composites derived from layered double hydroxide precursors, *J. Colloid Interface Sci.*, 2016, **481**, 144–157.

94 X. Sun, G. Liu, T. Shen, Y. Hu, Z. Song, Z. Wu, Q. Li, L. Zheng, W. Chen and Y. F. Song, Directional Activation of Oxygen by the Au-Loaded ZnAl-LDH with Defect Structure for Highly Efficient Photocatalytic Oxidative Coupling of Methane, *Small*, 2024, **20**, 2310857.

95 Z. Li, Q. Zhang, X. Liu, L. Wu, H. Hu and Y. Zhao, One-step mechanochemical synthesis of plasmonic Ag/Zn–Al LDH with excellent photocatalytic activity, *J. Mater. Sci.*, 2018, **53**, 12795–12806.

96 D. Li, L. Fan, Y. Shen, M. Qi, M. D. Ali, D. Liu and S. Li, Degradation of rhodamine B under visible-light by Cu-doped ZnAl layered double hydroxide, *J. Nanosci. Nanotechnol.*, 2019, **19**, 1090–1097.

97 C. R. Chen, H. Y. Zeng, M. Y. Yi, G. F. Xiao, R. L. Zhu, X. J. Cao, S. G. Shen and J. W. Peng, Fabrication of Ag_2O/Ag decorated ZnAl-layered double hydroxide with enhanced visible light photocatalytic activity for tetracycline degradation, *Ecotoxicol. Environ. Saf.*, 2019, **172**, 423–431.

98 D. Téllez-Flores, M. Sánchez-Cantú, F. Tzompantzi, A. G. Romero-Villegas, C. Tzompantzi-Flores, J. E. Carrera-Crespo, R. Pérez-Hernández and E. Rubio-Rosas, Influence of the Zn/Al molar ratio over the photocatalytic hydrogen production by ZnS/ZnAl-LDH composites, *Int. J. Hydrogen Energy*, 2025, **108**, 32–42.

99 Y. Yang, J. Li, T. Yan, R. Zhu, L. Yan and Z. Pei, Adsorption and photocatalytic reduction of aqueous Cr(VI) by Fe_3O_4-ZnAl-layered double hydroxide/TiO_2 composites, *J. Colloid Interface Sci.*, 2020, **562**, 493–501.

100 X. Li, Z. Yu, L. Shao, H. Zeng, Y. Liu and X. Feng, A novel strategy to construct a visible-light-driven Z-scheme (ZnAl-LDH with active phase/g-C_3N_4) heterojunction catalyst via polydopamine bridge (a similar "bridge" structure), *J. Hazard. Mater.*, 2020, **386**, 121650.

101 G. Mendoza-Damián, F. Tzompantzi, A. Mantilla, R. Pérez-Hernández and A. Hernández-Gordillo, Improved photocatalytic activity of SnO_2–ZnAl LDH prepared by one step Sn^{4+} incorporation, *Appl. Clay Sci.*, 2016, **121**, 127–136.

102 D. Wu, F. He, Y. Dai, Y. Xie, Y. Ling, L. Liu, J. Zhao, H. Ye and Y. Hou, A heterostructured ZnAl-LDH@ZIF-8 hybrid as a bifunctional photocatalyst/adsorbent for CO_2 reduction under visible light irradiation, *Chem. Eng. J.*, 2022, **446**, 137003.

103 T. Wang and Z. Jin, Graphdiyne (C_nH_{2n-2}) based CuI-GDY/ZnAl LDH double S-scheme heterojunction proved with in situ XPS for efficient photocatalytic hydrogen production, *J. Mater. Sci. Technol.*, 2023, **155**, 132–141.

104 G. Starukh, Photocatalytically enhanced cationic dye removal with Zn-Al layered double hydroxides, *Nanoscale Res. Lett.*, 2017, **12**, 391–398.

105 J. J. Gil, O. Aguilar-Martínez, Y. Piña-Pérez, R. Pérez-Hernández, C. E. Santolalla-Vargas, R. Gomez and F. Tzompantzi, Efficient ZnS–ZnO/ZnAl-LDH composite for H_2 production by photocatalysis, *Renewable Energy*, 2020, **145**, 124–132.

106 D. Behera, P. Priyadarshini and K. Parida, ZIF-8 metal–organic frameworks and their hybrid materials: emerging photocatalysts for energy and environmental applications, *Dalton Trans.*, 2025, **54**, 2681–2708.

107 N. Sultana, P. Priyadarshini and K. Parida, UiO-66-NH_2 and its functional nanohybrids: unlocking photocatalytic potential for clean energy and environmental remediation, *Sustainable Energy Fuels*, 2025, **9**, 3458–3494.